

SPITZER'S VIEW OF THE CANDIDATE CLUSTER AND PROTOCLUSTER CATALOG (CCPC)

J.R. FRANCK¹, S.S. MCGAUGH¹*Draft version January 23, 2017*

ABSTRACT

The Candidate Cluster and Protocluster Catalog (CCPC) contains 218 galaxy overdensities composed of more than 2000 galaxies with spectroscopic redshifts spanning the first few Gyrs after the Big Bang ($2.0 \leq z < 6.6$). We use *Spitzer* archival data to track the underlying stellar mass of these overdense regions in various temporal cross sections by building rest-frame near-infrared luminosity functions across the span of redshifts. This exercise maps the stellar growth of protocluster galaxies, as halos in the densest environments should be the most massive from hierarchical accretion. The characteristic apparent magnitude, $m^*(z)$, is relatively flat from $2.0 \leq z < 6.6$, consistent with a passive evolution of an old stellar population. This trend maps smoothly to lower redshift results of cluster galaxies from other works. We find no difference in the luminosity functions of galaxies in the field versus protoclusters at a given redshift, apart from their density.

Subject headings: galaxies: clusters: general - galaxies: high-redshift - galaxies: evolution

1. INTRODUCTION

The nascent study of protoclusters is at a juncture of two important evolutionary epochs in the universe: the early growth of large structures and the rapid assembly of galaxy mass at $z \geq 2$. Careful study of these objects can probe both cosmology and galaxy formation and evolution. The initial mass overdensities in the early universe (and their subsequent collapse) are governed by the cosmic matter density (Ω_m), σ_8 , and the cosmological constant Ω_Λ . Thus, by examining their properties (mass, evolutionary state) and number density of these early structures, they can provide constraints on these cosmological parameters. The tracers of these overdense structures (i.e., galaxies) can be used to investigate the role environment plays in their growth and evolution. Formation models of galaxies must match observations across both cosmic time and throughout space to be considered viable. More simply, void and cluster galaxies must both be reproduced for all $z \geq 0$. The focus of this work will be primarily on the properties of galaxies in dense environments, but this juncture of structure and galaxy evolution are clearly relatable in many ways.

It has been clear for many decades that galaxies at $z = 0$ have varied properties that correlate strongly with density in the well-established morphology-density relation (Dressler 1980; Balogh et al. 2004). Galaxies in dense environments show clear evolution at higher redshift (Butcher & Oemler 1984), in that there are more passive galaxies in local clusters, but a greater fraction of star forming objects in higher redshift systems. This can be seen observationally in the fraction of quiescent, ‘red-sequence’ objects in contrast with the ‘blue cloud’ of star forming galaxies (SFGs) as a function of redshift (Stanford et al. 1995; Rakos & Schombert 1995). These two facts provide an initial scaffolding from which galaxy evolutionary models can be wrought: quiescent systems dominate high density regions of the local universe, and this need not hold throughout cosmic time. What is the

path that must be taken to satisfy these two simple observations?

One prescription to turn these observational facts into a coherent model is to identify physical processes that effectively turn SFGs into quiescent systems preferentially in dense environments. Commonly invoked interactions are ram-pressure stripping of cold gas by the intracluster medium (ICM; Gunn & Gott 1972), removal of the hot gas halo of a galaxy to halt the cooling of gas to sustain star formation (e.g. strangulation; Larson et al. 1980), galaxy-galaxy interactions that disrupt the galaxy (Moore et al. 1996), and a variety of others. The overarching umbrella that is used to refer to these proposed mechanisms is called ‘quenching’ (Peng et al. 2010), loosely defined here as the environmental process(es) that abruptly discontinue star formation in a galaxy.

Each proposed quenching process has a distinct time scale at which it can effectively halt star formation. These are generally related to the crossing/dynamical time of the galaxies interacting with other galaxies and/or the ICM. For this latter case, it also assumes that the hot ICM is in place at the epoch in question so as to produce the desired effect. These quenching timescales have been estimated to operate on the order of a few Gyrs for an effective change to manifest itself (Brodwin et al. 2013). If cluster galaxies are transformed primarily by one quenching mechanisms, it might be possible to examine the galaxy populations in clusters at various cross-sections in time (e.g., redshifts) to isolate the process responsible.

Another proposed scenario used to explain the evolution of the galaxy population in clusters is from galaxy mergers. Hierarchical accretion suggests that galaxies assemble from the bottom up. In the context of clusters, these mergers have been proposed to be either dry (e.g. gas-free; van Dokkum 2005) or wet (gas-rich collisions; Faber et al. 2007). In the wet merger scenario, two or more blue cloud galaxies come together in a burst of star formation, turning into a spheroidal configuration (Mihos & Hernquist 1996), and are then quenched via some

¹ Case Western Reserve University, 10900 Euclid Ave., Cleveland, OH 44106

mechanism. This is effectively a transition from the blue cloud onto the red sequence. Dry mergers, on the other hand, push galaxies along the red sequence as they grow in stellar mass, but remain with a generally passive stellar population (color). It is possible and even probable that the various quenching mechanisms and merger scenarios could all play a role of varying importance. Do any observations hint at a timescale of rapid development in the history of cluster galaxies?

The red sequence feature of galaxy clusters has been historically used as a tracer of the core galaxy population at redshifts $z < 1.5$ (Stanford et al. 1995; Rakos & Schombert 1995; Stanford et al. 1998; Eisenhardt et al. 2008; Mei et al. 2009). Using models of galaxy colors a mean stellar age of the individual systems can be estimated. Progenitor bias (van Dokkum & Franx 2001) can ultimately lead to an increased estimated formation redshift (z_f) for a cluster’s galaxy population as a whole. Despite this caveat, the stellar age of the brightest systems on the red sequence can give some indication as to when the most massive galaxies formed their stars. Models of galaxy growth used to match the evolution of the red sequence feature typically rely on pure, passive evolution models that were formed in a single burst at high redshift $z_f > 3$ (Eisenhardt et al. 2008). In fact, some studies of clusters suggest even larger formation redshifts of $z_f > 5$ (Rakos & Schombert 1995; Schombert & Rakos 2009). As the redshift of the cluster sample increases, the formation redshift also grows (with an accompanying increase of scatter).

For instance, for cluster redshifts $z > 1$, it appears that $z_f = 30$ is not ruled out (Fig 19 of Eisenhardt et al. 2008). Not all cluster galaxies need form at $z_f > 5$, but at least some passive systems were born remarkably early in the universe. This could simply be a manifestation of galaxy downsizing (Cowie et al. 1996), in which the largest stellar mass galaxies (presumably formed in the densest regions) formed earlier in the universe. Within the literature, there is no consensus for any single model or mechanism for the redshift evolution of the red sequence feature (Fassbender et al. 2014; Fritz et al. 2014).

By shifting the focus from the highly biased red sequence galaxies to cluster populations in general, there is the hope that the bulk stellar properties of these systems could be investigated as a function of redshift. Mancone et al. (2010) mapped the luminosity functions (LFs) of cluster galaxies spanning $0.3 < z < 2.0$ at *Spitzer* wavelengths. At the highest redshift of this sample, *Spitzer* $3.6 \mu\text{m}$ coverage measures rest-frame J band, which is a tracer of the stellar population for a range of ages. They mapped the evolution of the characteristic luminosity $m^*(z)$ ² of the clusters by comparing the data to models of simple stellar populations with various formation redshifts z_f . This is similar to the exercise performed for red-sequence fitting. The mean formation age of these systems was $z_f \sim 2.5$ (Mancone et al. 2010), with the same behavior noted previously: higher redshift clusters favor higher formation redshifts. Their two highest redshift bins ($z \geq 1.5$) have $m^*(z)$ values nearly a magnitude fainter than the predicted evolution of their best

fitting model (their Fig 7). The conclusion drawn from this observation is that rapid mass assembly (up to $4\times$ growth) must occur in cluster galaxies $z \leq 1.5$ (Mancone et al. 2010). Brodwin et al. (2013) investigated the star formation activity of galaxies in these clusters to look for clues as to the nature of this mass assembly. They found that the star formation within the core of these clusters transition from unquenched to quenched at the same epoch ($z \sim 1.4$) as the rapid assembly era within Mancone et al. (2010). This behavior is generally attributed to wet mergers within the cluster core, rapidly growing the mass of these systems and then abruptly turning off the star formation activity.

In the previous examples, all of the structures were considered to be clusters. Generally speaking, the highest redshift at which virialized halos of $M \geq 10^{14} M_\odot$ (e.g. clusters) are expected is at $z \sim 2$ in large ΛCDM simulations (Chiang et al. 2013). The collection of components that will constitute a cluster in the future is referred to as a protocluster. Observationally, galaxy overdensities at $z > 2$ are designated as protoclusters for the sake of simplicity, as it is difficult to confirm these systems to be in virial equilibrium apart from a handful of cases (Gobat et al. 2011; Wang et al. 2016). This unique transition point in the universe represents an epoch at which galaxies could first begin to interact with one another. Mancone et al. (2010) and Brodwin et al. (2013) presented tantalizing evidence that the majority of mass assembly occurred around $z \sim 1.5$, but higher redshift luminosity functions of structure might yield further insight into the galaxy growth within dense environments.

Wylezalek et al. (2013) identified *Spitzer* galaxy overdensities around high redshift ($1.3 < z < 3.1$) radio-loud AGN and built 3.6 and $4.5 \mu\text{m}$ LFs in Wylezalek et al. (2014). This redshift range overlapped the sample of Mancone et al. (2010) and extended the age probed by more than 1 Gyr. Remarkably, the $m_{3.6}^*$ and $m_{4.5}^*$ evolution over the redshifts probed are well fit by a passive stellar evolution model formed at $z_f = 3$ or larger. They also do not match the results of Mancone et al. (2010), in that they fail to see a burst of mass assembly at $z \leq 1.5$. This is attributed to a sampling bias, in that the high redshift overdensities are thought to be the most massive, rare systems in the universe, while the lower redshift sample is tracing the growth of less massive clusters. This is analogous to galaxy downsizing, in that the most massive overdensities are fated to assemble into a cluster mass halo more quickly in ΛCDM (Chiang et al. 2013). Therefore, signatures of mass assembly for the progenitor systems of (Wylezalek et al. 2014) could potentially be observable beyond their redshift limit of $z \approx 3$. In Section 3, we probe these earlier epochs to possibly identify epochs at which rapid mass growth or quenching might be exhibited.

Thus far, it appears that galaxies within clusters, as traced by both red sequence and LF models, form at high redshift ($z_f \geq 3$) and evolve passively thereafter. This is an interesting result, as the cosmic star formation rate in the universe does not peak until approximately $z \sim 2$ (Madau & Dickinson 2014). Indeed, if galaxies in dense environments form earlier than their ‘field’ galaxy counterparts, which follow the mean trend, then evidence of this should be apparent at high redshifts. The number of spectroscopically confirmed protoclusters has evolved

² We designate the characteristic magnitude in lower case (m^*) to emphasize that it is a measure of the apparent magnitude and to distinguish it from the stellar mass (M_*) also found in this text.

considerably after the first few discoveries (Steidel et al. 1998; Venemans et al. 2002), but were still only numbered in the few dozens up until recently. These were also identified by a wide range of selection techniques, from blind spectroscopic surveys (Steidel et al. 1998) to targeted narrowband (NB) imaging around high redshift quasars (Venemans et al. 2007). In the instances in which these galaxy overdensities were compared with field galaxies at a similar redshift, the results of environmental evolution are varied at best. We continue the exploration of these results at higher redshift in Section 4.

The majority of cases in the literature where protocluster galaxies were measured with respect to field sources consist of one or two candidate structures that are compared to a ‘blank’ field-of-view. For instance, Casey et al. (2015) studied a protocluster at $z = 2.5$ within the COSMOS field and found that it had evidence of greater AGN activity, more indications of merging/interacting galaxies, and a population of Lyman-Break Galaxies (LBGs) with $\sim 1.5\times$ greater stellar mass. These had similar star formation rates (SFRs) when compared to field sources, though. For other protoclusters at $z \leq 2.5$ identified with NB filters centered on the redshifted $H\alpha$ line, the candidate galaxies were also found to be dustier (Cooke et al. 2014), more massive, and not significantly forming more stars than their field counterparts (Hatch et al. 2011).

Similar studies that trace the $Ly\alpha$ emission of protocluster galaxies find that they are generally brighter (Zheng et al. 2016), less dusty (although this may be a selection effect), and younger (Dey et al. 2016). $Ly\alpha$ equivalent widths (EWs) have been used extensively as an estimator for the star formation rate of galaxies in the high redshift universe (Dijkstra & Westra 2010), and Zheng et al. (2016) find evidence that the EWs are stronger at $z = 2.8$. Dey et al. (2016) do not find such EW dependence at $z = 3.8$, while Toshikawa et al. (2016) finds smaller EW_0 in a protocluster at $z = 3.67$ when compared to the field. Hayashi et al. (2011) and Hayashi et al. (2012) find only the reddest galaxies in their structures have statistically significant environmental dependence. It seems clear that when individual high redshift structures are analyzed, usually an environmental influence is found, but the effect is varied. It is also apparent that in some protoclusters, the property in question is enhanced (e.g. dustier galaxies), while in others it is diminished, even at similar redshifts.

This does not seem to be the case when multiple candidate structures are identified in the same manner, or large surveys are systematically analyzed. Ownsworth et al. (2016) used a constant number density selection technique for the UKIDSS survey to measure the evolution of galaxies. This selection technique is thought to be much less-biased when compared with a mass-limited selection in matching progenitor galaxies to their offspring. Their results point to a relatively early formation redshift ($z \geq 3$ and possibly earlier) and subsequent passive evolution with little environmental influence. With a similar method, Zhao et al. (2016) tracked the growth and evolution of $z = 0$ Brightest Cluster Galaxies (BCGs) from $z \sim 2$. A key result is that most of the mass growth must occur at $z < 2$, as BCGs are not divergent from similar mass systems. Diener et al. (2013, 2015) identified more than 40 spectroscopic galaxy group and larger systems in the COSMOS field. Compared to field sources, their

analysis revealed no statistically significant color (stellar population) difference in the group environments with respect to the field.

This begs the question of why overdensities do not show up as significant deviations from their field counterparts when analyzed systematically at a variety of redshifts, while individual systems have found statistically different evolution over similar epochs. It is often difficult to match the results of these protocluster studies coherently. These protoclusters exist at a wide range of redshifts, each within their infancy and characterized by the rapid changes expected in a Λ CDM universe (Chiang et al. 2013; Muldrew et al. 2015). Particularly for the individual case studies (Hatch et al. 2011; Hayashi et al. 2012; Cooke et al. 2015; Dey et al. 2016; Zheng et al. 2016), different instruments and selection techniques were used, which targeted different populations of galaxies. Furthermore, the galaxy properties themselves were not all analyzed in the same manner.

In an attempt at tackling the complex problem of galaxy evolution, it can be helpful to simplify the approach (Abramson et al. 2016), and confront the issue in a new way instead of adding further epicycles. It was this impetus that inspired us to construct the Candidate Cluster and Protocluster Catalog (hereafter CCPC; Franck & McGaugh 2016b,a). With a straightforward algorithm, we were able to systematically detect galaxy overdensities from disparate spectroscopic catalogs in the high redshift universe. Then, the properties of the galaxies within these candidate structures can be traced through cosmic time in a series of cross-sections. We hope to address the evolution of galaxy stellar mass, as Mancone et al. (2010) and Wylezalek et al. (2014) did at lower redshifts, while simultaneously mapping the field evolution in a consistent manner over a range of redshifts. Although not a longitudinal study, these snapshots of galaxies in dense environments may provide a powerful glimpse into the behavior governing their evolution.

We present here a detailed analysis of the CCPC sample to date using *Spitzer* IRAC and supplementary *Hubble Space Telescope* near-infrared (NIR). In this back-to-basics approach, we measure the 3.6 and 4.5 μm LFs of the galaxies in the CCPC as a function of redshift. This serves as a tracer of the stellar mass of these objects, and are compared with ‘field’ galaxies identified in the same spectroscopic surveys used for the CCPC.

Throughout this work we assume a cosmology of $\Omega_m = 0.3$ and $\Omega_\Lambda = 0.7$, with a Hubble value of $H_0 = 70 \text{ km s}^{-1} \text{ Mpc}^{-1}$. All magnitudes quoted are in the AB system, with apparent magnitudes in the four *Spitzer* IRAC channels denoted as [3.6], [4.5], [5.8], and [8]. The accompanying apparent magnitudes from *Hubble Space Telescope* measurements will be referred to by the filter name (e.g. $F160W$).

2. OBSERVATIONS

The CCPC identifies structure around galaxies by mining archival spectroscopic redshift catalogs. Any volume within a search radius of $R = 20$ comoving Mpc (cMpc) and distance in redshift space Δz corresponding to ± 20 cMpc which contains 4 or more galaxies and display a galaxy overdensity of $\delta_{gal} > 0.25$ is considered a candidate system (Franck & McGaugh 2016b,a). These are

the minimum requirements and, in many cases, are exceeded.

The algorithm was designed to be used on a variety of survey depths and widths, where $N \geq 4$ is used as a signpost from which the volume overdensity can be computed. The average number density of these systems is $n \sim 0.05 \text{ cMpc}^{-3}$, and a mean galaxy overdensity of $\delta_{gal} \sim 2.0$. We have shown in [Franck & McGaugh \(2016b\)](#) and [Franck & McGaugh \(2016a\)](#) that these protocluster candidates are statistically distinct both spatially and along the line of sight from non-CCPC galaxies.

2.1. Galaxy Selection

The catalog contains a total of 216 structures spanning $2 < z < 6.56$. We include two objects of interest at $z = 6.56$ from [Franck & McGaugh \(2016a\)](#) to bring the total number of candidate systems to 218. These systems lack field galaxies, and so a galaxy overdensity (δ_{gal}) cannot be computed, a requirement for inclusion in the CCPC. In this list there exist 2048 galaxies. The vast majority of these objects are identified either by spectroscopically targeting Lyman Break Galaxies (LBGs [Steidel et al. 1998](#)) or follow-up spectroscopy on suspected $H\alpha/Ly\alpha$ emitters from NB imaging ([Venemans et al. 2007](#)).

We note here briefly that SFGs are not the dominant massive galaxy population at these epochs. In the high redshift universe, [van Dokkum et al. \(2006\)](#) estimated that only 20% of all galaxies with $M_* > 10^{11} M_\odot$ are LBGs. The majority of systems ($\sim 70\%$) are thought to be Distant Red Galaxies (DRGs), which are often too faint in the observed optical passbands to be spectroscopically targeted. They can also lack the strong emission lines of their unobscured star-forming counterparts. We will discuss further implications of this in Section 4.

2.2. Data

All of the measurements in this work came from archival data sets. The *Spitzer* Heritage Archive provided nearly 600 processed images in all four IRAC channels covering most of the CCPC fields. The greatest wavelength coverage of these systems came from the first two channels (3.6 and 4.5 μm), with galaxy contributions from 177 and 184 CCPC structures, respectively. Nearly $\sim 75\%$ of the 2048 CCPC galaxies were measured at 4.5 μm . All photometry was performed using 2" radius apertures using the IRAF³ ([Tody 1986, 1993](#)) QPHOT package, and the magnitudes were computed by $m_{AB} = 23.9 - 2.5 \log(f_\nu/1\mu\text{Jy})$. Aperture corrections were applied to each galaxy (0.32 mags in [3.6] and 0.36 for [4.5]), as in [Papovich et al. \(2010\)](#). Our photometry is consistent with the reported [3.6] and [4.5] AB magnitude values compiled in the 3D-HST database ([Skelton et al. 2014](#)) within the CANDELS fields, apart from the aperture corrections.

We obtained more limited data coverage of the CCPC with the *Hubble Space Telescope* in the *F160W* bandpass

via the *Hubble Legacy Archive*. The scope of these images were primarily concentrated within the CANDELS fields ([Grogin et al. 2011](#)). Approximately 25% of the CCPC was measured within these images. Fluxes were measured in apertures of radius 0.4" with a zeropoint magnitude of 25.75, values which were adopted from the WFC3 Handbook. The pixel scale of these images ranged from ~ 7 to 33.33 pix/".

With *Hubble Space Telescope* and *Spitzer* data, there were cases in which a galaxy was measured in a number of images. All magnitudes listed here are the uncertainty-weighted mean value of the photometry.

2.3. Building the Luminosity Function

We map the evolution of the CCPC galaxy luminosity function using the [Schechter \(1976\)](#) form

$$\phi(L)(dL) = \phi^* \left(\frac{L}{L^*} \right)^\alpha e^{-L/L^*} \frac{dL}{L^*}, \quad (1)$$

which relates the characteristic number density ($\phi(L)$) of sources over a range of luminosities. L^* is the characteristic luminosity of the distribution where the number density decreases rapidly, and α is the slope of the faint end. The scaling factor of the Luminosity Function is ϕ^* . In this work, we will adopt the magnitude functional form of

$$\phi(m) = 0.4 \ln(10) \phi^* \frac{10^{0.4(m^* - m)^{\alpha+1}}}{\exp[10^{0.4(m^* - m)}]}. \quad (2)$$

To construct the distribution function, we first compute the density of each candidate structure by finding the minimum rectangular region (in units of arcmin^2) that bounds all galaxies. We then place galaxies in magnitude bins of $\Delta m = 0.4$ for a given redshift range, and finally divide this by the summed surface area of candidates at that redshift. The uncertainty for each magnitude bin is the 1σ photometric uncertainty of the galaxy magnitudes in that bin. The number density uncertainty is Poissonian (\sqrt{N}). The redshift bins were designed to offer a balance between similar temporal spacing and number of galaxies at each epoch. This balance is necessary, for if the time period probed by each snapshot is too variable or too large, then any evolutionary inferences that the luminosity function might provide could be lost. In addition, too few galaxies in a redshift bin can be insufficient in fitting the parameters of the Schechter function. We aim for $N \geq 10^2$ galaxies per redshift bin whenever possible, as this provides a robust fit to the data in practice.

We computed the e - and k - corrections of each galaxy by estimating (using EzGal; [Mancone & Gonzalez 2012](#)) the observed magnitude difference of a BaSTI simple stellar population model ([Percival et al. 2009](#)) between the model's magnitude at the observed redshift of the galaxy and the center of its redshift bin. Typically these corrections are less than $\Delta m \sim 0.05$ magnitudes, which are smaller than our photometric uncertainties. There is no net change in the values of m^* when the corrections are applied, as these shifts in magnitude are balanced out by the galaxies at either end of the redshift bin.

For fitting the Schechter function to the data, we used SciPy's *curvefit* routine. This routine takes the data table, the Schechter function, the parameters to be fit and

³ IRAF is distributed by the National Optical Astronomy Observatories, which are operated by the Association of Universities for Research in Astronomy, Inc., under cooperative agreement with the National Science Foundation.

a set of initial guesses for those parameters. These initial input values are insensitive to the outcome. The solution to Equation 2 is optimized via a Levenberg-Marquardt algorithm. In practice, if the data have sufficient depth to fit the faint-end slope α , all three parameters can be solved for simultaneously, as Wylezalek et al. (2014) were able to do. However, the variability of our data depth does not permit us to reliably fit α at all redshifts, and we therefore set it as a constant $\alpha = -1$. This is standard procedure for *Spitzer* LFs of insufficient depth (Mancone et al. 2010). Wylezalek et al. (2014) obtained the same results independently of whether α was fixed or not. The selection function of spectroscopic surveys used to construct the CCPC will typically favor bright galaxies out of necessity, which would artificially restrict the faintest regions in magnitude space, regardless.

The main science goal of these LFs is to investigate the temporal evolution of $m^*(z)$ and number density of the largest galaxies in these systems, and so the faint slope of the galaxies is of relatively minor importance. Even at low redshifts, determining α can be problematic, as low surface brightness galaxies are often missed (McGaugh 1996). When the value of α is allowed to vary, it is generally consistent with $\alpha \approx -1$ within the uncertainties for the lowest redshift sources in our data. At higher redshifts, there are too few galaxies in the faint magnitude bins from incompleteness, and the fitting routine breaks down. In short, the optimization procedure of *curvefit* provides a more robust fit to the data with a constant $\alpha = -1$. There have been no completeness corrections implemented on the data set. The focus of this research is on tracing the brightest, most massive galaxies at a given epoch. Attempting to adjust the number of faint galaxies is (1) not important in achieving the research aim and (2) uncertain at best, as spectroscopic surveys of high redshift sources are inherently biased in this regard.

Once the fitting routine has provided values of m^* and ϕ^* , the uncertainties are calculated via bootstrapping. The galaxies in each redshift bin are resampled with replacement 10^4 times. Each instance is fitted to Eq 2 in the same manner as the full data set. The 95% confidence region of the data is provided by fitting the $\pm 2\sigma$ values of m^* . Figure 1 illustrates this.

3. RESULTS

3.1. Luminosity Functions

Table 1 and Table 2 contain the [3.6] and [4.5] *Spitzer* parameters estimated for the CCPC, respectively. In general, the values of m^* are flat as a function of redshift, suggesting little evolution. Figure 1 shows a Luminosity Function for a single epoch to illustrate the finer details of the fit. Figure 2 shows the full set of Luminosity Functions at each epoch at 3.6 μ m, while Figure 3 does the same for [4.5].

3.2. Field Luminosity Functions

In an effort to compare galaxies in overdense environments with their ‘field’ counterparts, we assembled a list of all spectroscopic galaxies that were in the same surveys as the protoclusters in our sample. This list contains more than 4000 galaxies, double the number of the CCPC ($N = 2048$ objects). We imposed no richness or density

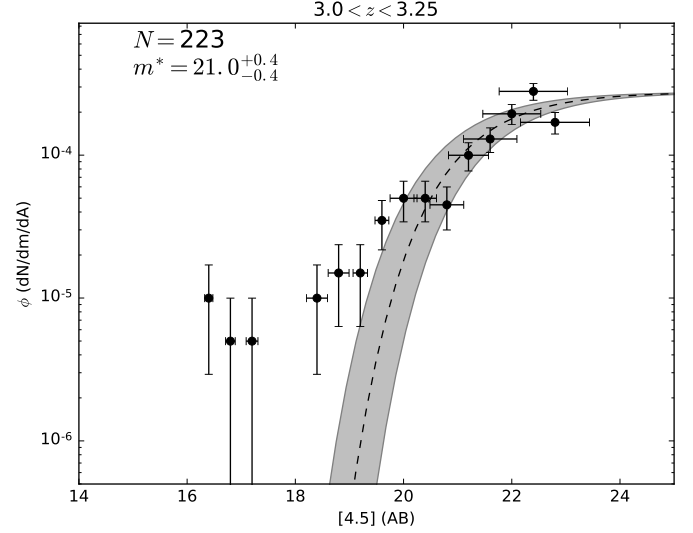


Figure 1. The 4.5 μ m Luminosity Function of CCPC galaxies at redshifts $3.0 \leq z < 3.25$. ϕ is the number of galaxies at a specific magnitude per square arcminute ($dN/dm/dA$). Uncertainties in the number density of sources are Poissonian ($\sqrt{N(dm)}$), while the magnitude uncertainties in each bin are the average uncertainty of the bin’s galaxies. SciPy’s *curvefit* routine’s best fit to the data is the black dashed line. The number of galaxies in the plot and the value of m^* and its 2σ bootstrapped uncertainties are listed in the top left corner. In this work, α is defined to be -1. The gray shaded area represents the 95% bootstrapped confidence region of the fit.

Table 1
3.6 μ m CCPC Luminosity Function

Redshift Range	N Galaxies	m^* (AB)	$2\sigma(m^*)$ (95% CI)	ϕ^* ($dN/dm/dA$)
$2 \leq z < 2.25$	192	20.01	+0.50 -0.65	2.94×10^{-4}
$2.25 \leq z < 2.5$	159	20.89	+0.88 -0.68	3.41×10^{-4}
$2.5 \leq z < 2.75$	110	21.13	+0.67 -0.96	3.39×10^{-4}
$2.75 \leq z < 3$	205	21.42	+0.46 -0.33	5.01×10^{-4}
$3 \leq z < 3.25$	186	21.06	+0.60 -0.65	2.74×10^{-4}
$3.25 \leq z < 3.5$	77	21.07	+1.22 -1.47	2.05×10^{-4}
$3.5 \leq z < 4$	68	20.51	+0.63 -0.99	1.34×10^{-4}
$4 \leq z < 5$	117	21.06	+0.38 -0.49	1.75×10^{-4}
$5 \leq z < 6.6$	54	21.83	+0.74 -1.23	6.30×10^{-4}

Note. — The results of fitting a Schechter function (Equation 2) to the CCPC galaxies in a series of redshift bins (1st column). The number of galaxies (N) in each redshift bin is listed in the 2nd column, followed by the fitted m^* parameter in the 3rd column. The 4th column represents the 95% confidence interval of the m^* value. This uncertainty was computed by bootstrapping with resampling of the data. The characteristic density (ϕ^*) in units of the number of galaxies per magnitude bin per square arcminute is found in the final column. The faint end slope of the LF was fixed to be $\alpha = -1$.

criteria on this sample set, apart from that its members were not within the volume of a candidate protocluster. Although some of these galaxies may exist in a volume with $N \geq 4$ galaxies (a requirement for CCPC candidacy), they did not have the sufficient galaxy density to be flagged as a protocluster candidate. The references to the spectroscopic measurements of the field systems are

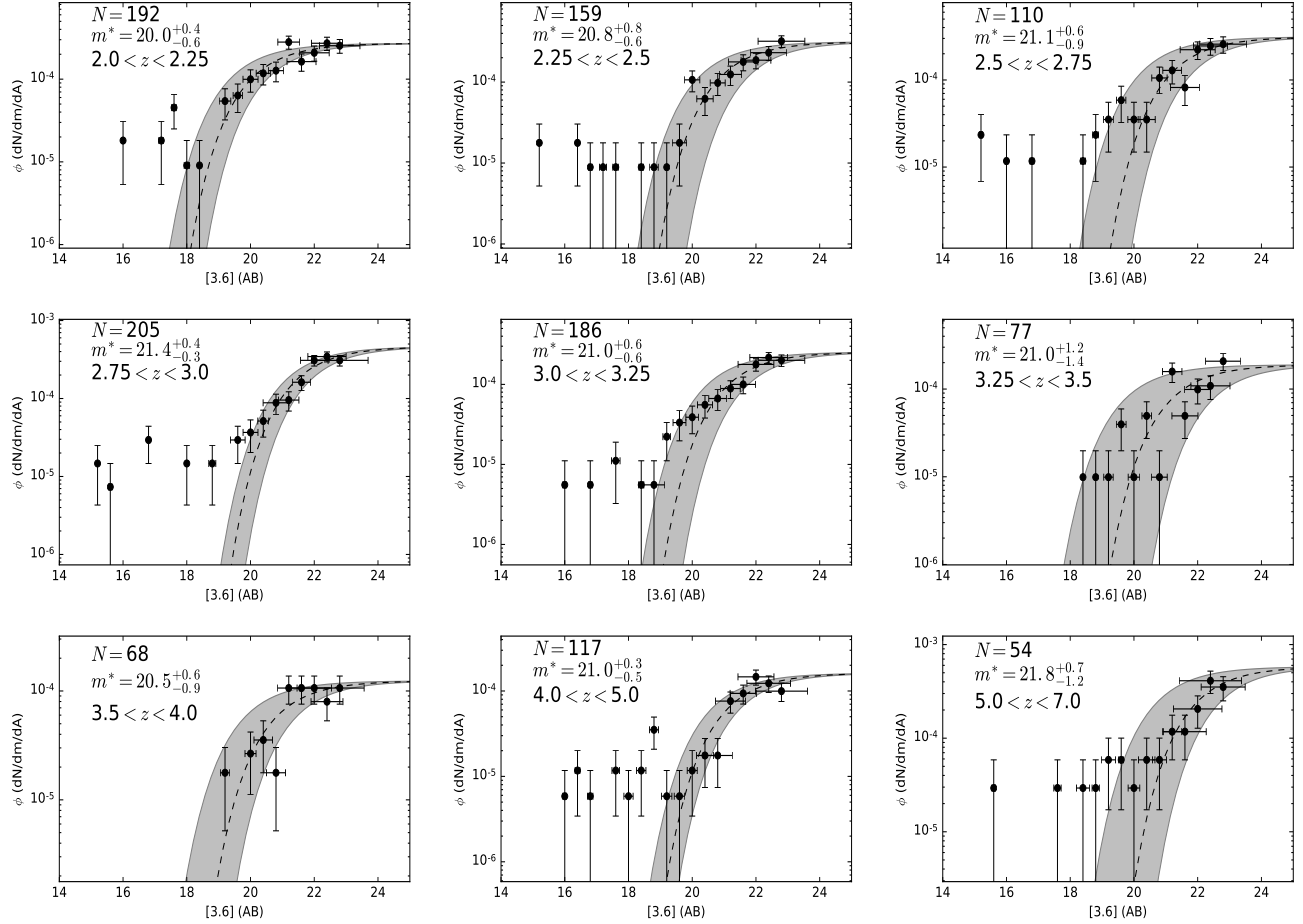


Figure 2. The $3.6\mu\text{m}$ *Spitzer* Luminosity Function at nine epochs across $2 \leq z < 7$. The surface number density (ϕ) of galaxies is measured in square arcminutes. The number density uncertainty is calculated by the root N value in each bin, while the magnitude uncertainties are the average photometric errors in that bin. The gray shaded regions are the 95% confidence intervals calculated by bootstrapping. The Schechter fit (Eq 2) to the CCPC data is the black dashed line, with α defined as -1. The number of galaxies and the value of m^* are listed in the upper left hand corner. The m^* uncertainties are the bootstrapped 2σ values. Galaxies much brighter than m^* we refer to as ‘hyperluminous’ sources and will be discussed in Section 4.

Table 2
4.5 μm CCPC Luminosity Function

Redshift Range	N Galaxies	m^* (AB)	$2\sigma(m^*)$ (95% CI)	ϕ^* (dN/dm/dA)
$2 \leq z < 2.25$	210	19.73	+0.56 -0.59	2.65×10^{-4}
$2.25 \leq z < 2.5$	180	20.27	+0.56 -0.53	3.35×10^{-4}
$2.5 \leq z < 2.75$	124	21.25	+0.58 -0.97	3.14×10^{-4}
$2.75 \leq z < 3$	249	21.36	+0.39 -0.31	5.13×10^{-4}
$3 \leq z < 3.25$	223	21.08	+0.41 -0.46	3.00×10^{-4}
$3.25 \leq z < 3.5$	108	21.31	+0.71 -0.80	2.76×10^{-4}
$3.5 \leq z < 4$	83	20.38	+0.51 -0.74	1.21×10^{-4}
$4 \leq z < 5$	117	20.71	+0.35 -0.74	1.68×10^{-4}
$5 \leq z < 6.6$	58	21.75	+1.97 -1.38	5.69×10^{-4}

Note. — Identical to Table 1, but at 4.5 μm .

located in the Appendix, and can also be found in the references of Franck & McGaugh (2016b) and Franck & McGaugh (2016a).

We analyzed these galaxies in the same manner and built an ‘All Galaxy’ LF (as a proxy for field galaxies) at each redshift bin. The value of ϕ^* was scaled to the CCPC LF at each epoch. As can be seen in Figs 4 and

5, the number density of field galaxies (red points) in all bins, at all epochs, are consistent with the CCPC $\phi(m)$ (black points). Fitting a Schechter function to ‘All Galaxies’ produces equivalent values of $m^*(z)$ to that of the CCPC galaxies, as can be seen by the overlapping 95% confidence intervals (red and gray shaded regions, respectively).

The CANDELS GOODS-S field is the deepest, most continuous spectroscopic survey from which dozens of structures are identified in our sample (Franck & McGaugh 2016b,a). Nearly 25% of galaxies in the CCPC originate in this field. To minimize the effects of varying spectroscopic selection functions from the heterogeneous sample the CCPC is constructed from, we constructed GOODS-S LFs for CCPC and non-CCPC galaxies. The m^* values remain unchanged at all redshifts in this subsample, for both field and overdense galaxies, within the uncertainties. Although spectroscopic selection is not definitively ruled out as a variable for the entirety of the CCPC LFs, it does not appear to be a driving factor in the CANDELS GOODS-S data.

As a further test, we limited our analysis to galaxies in the ‘All Galaxy’ list that had $N < 4$ galaxies within the CCPC search volume ($R = 20$ cMpc, $\Delta z \pm 20$ cMpc).

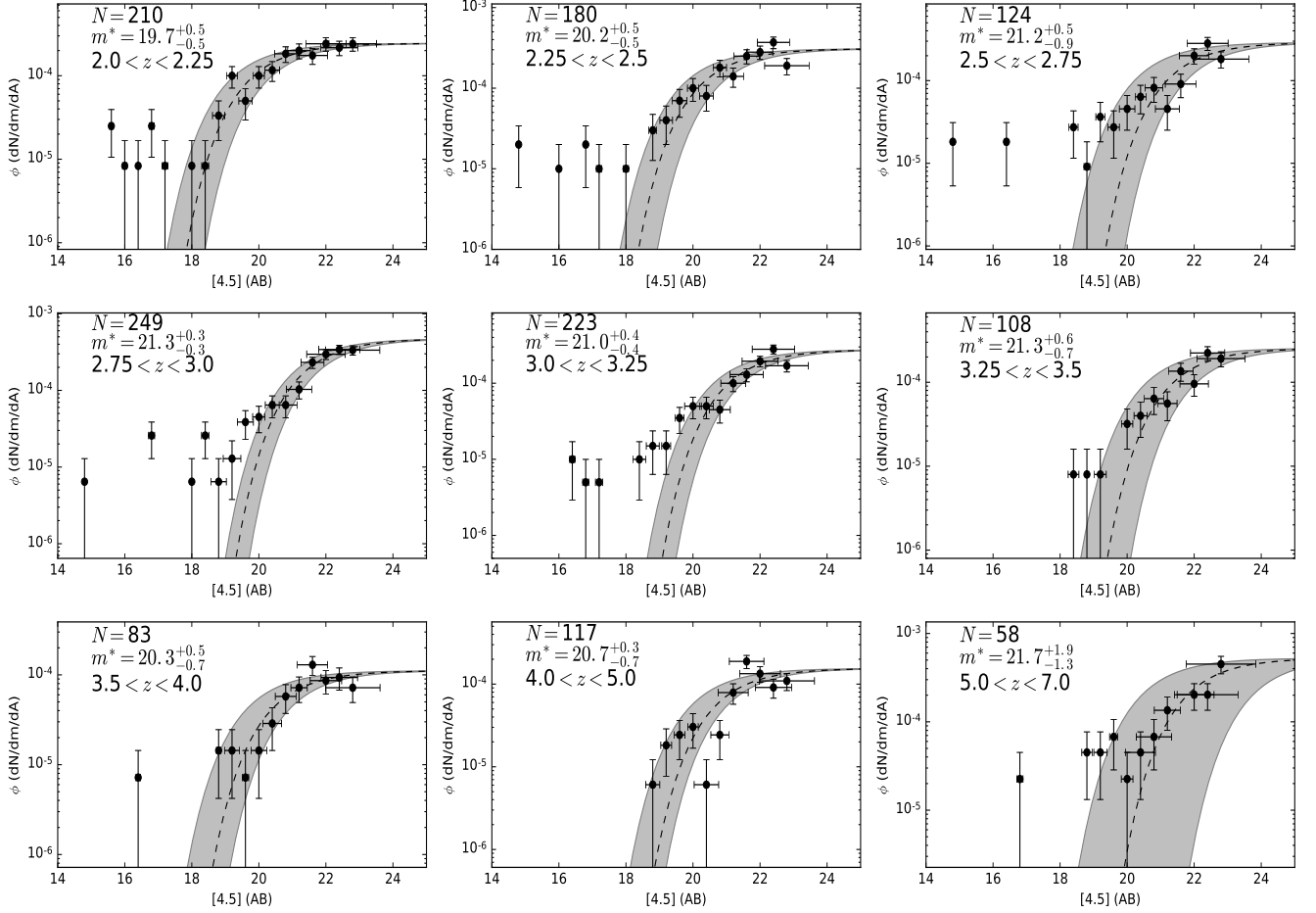


Figure 3. The $4.5\mu\text{m}$ version of Figure 2.

Although this ‘Reduced Field Galaxy’ sample limited the number of galaxies to 2299, this list is still larger than the number of CCPC galaxies, and thus remains a fair comparison. Interestingly, this imparted no measurable difference when compared to the shape of the ‘All Galaxy’ or CCPC LFs. It is possible that at these very early epochs, the galaxies that are spectroscopically selected have not had sufficient time to interact in their modestly dense environments and thus differentiate themselves. Another plausible explanation is that many of the galaxies selected in the overdense volumes are not future cluster galaxies, but rather are field interlopers that will disperse by $z = 0$ and thus show little/no differentiation from our field sample. These results will be discussed in more detail in Section 4.

3.3. Galaxy Colors

A selection tool used to identify high-redshift ($z > 1.3$) galaxies with *Spitzer* is the popular $[3.6] - [4.5] > -0.1$ color cut (Papovich et al. 2012; Wylezalek et al. 2014). It is a simple and effective way of removing low redshift galaxies from a sample, regardless of the underlying stellar population. Interestingly, more than 1/3 of the CCPC sample (all with spectroscopic redshifts $z > 2$) failed this color cut. Within the photometric uncertainties, many of these systems emit ‘true’ colors that would satisfy the criterion. However, this blind cut can remove a significant portion of a sample of high redshift

galaxies. This is not unique to our photometry. The galaxies in CCPC structures that are coincident with objects in the 3D-HST database (Skelton et al. 2014) show a similar result, with 33.8% of more than 300 galaxies having $[3.6] - [4.5] < -0.1$, with a median color of $[3.6] - [4.5] = -0.25$. This is a further piece of evidence suggesting that this aberrant fraction is the result of photometric uncertainty that has scattered the colors below the cut. There is no obvious correlation with apparent magnitude, therefore AGN or hyperluminous source contamination is likely not an issue.

Although effective at measuring the underlying stellar mass of high redshift galaxies from their rest-frame NIR emission, the colors of *Spitzer* are not sensitive to different stellar populations (Cooke et al. 2014). Even at the highest redshift of the CCPC ($z = 6.56$), the rest-frame wavelength observed at $4.5\mu\text{m}$ falls at just 5900\AA . As the majority of these galaxies were spectroscopically targeted as UV bright, star forming systems, it stands to reason that they should have blue colors, which *Spitzer* is not sensitive to. The *Hubble Space Telescope* WFC3 F160W filter probes rest-frame wavelengths of $2100 - 5300\text{\AA}$ between the redshift range $2.0 < z < 6.56$. Figure 6 illustrates the redshift evolution of the $F160W - [4.5]$ galaxy color as a function of redshift for a variety of stellar population models (Bruzual & Charlot 2003; Percival et al. 2009), with different initial mass functions (Chabrier

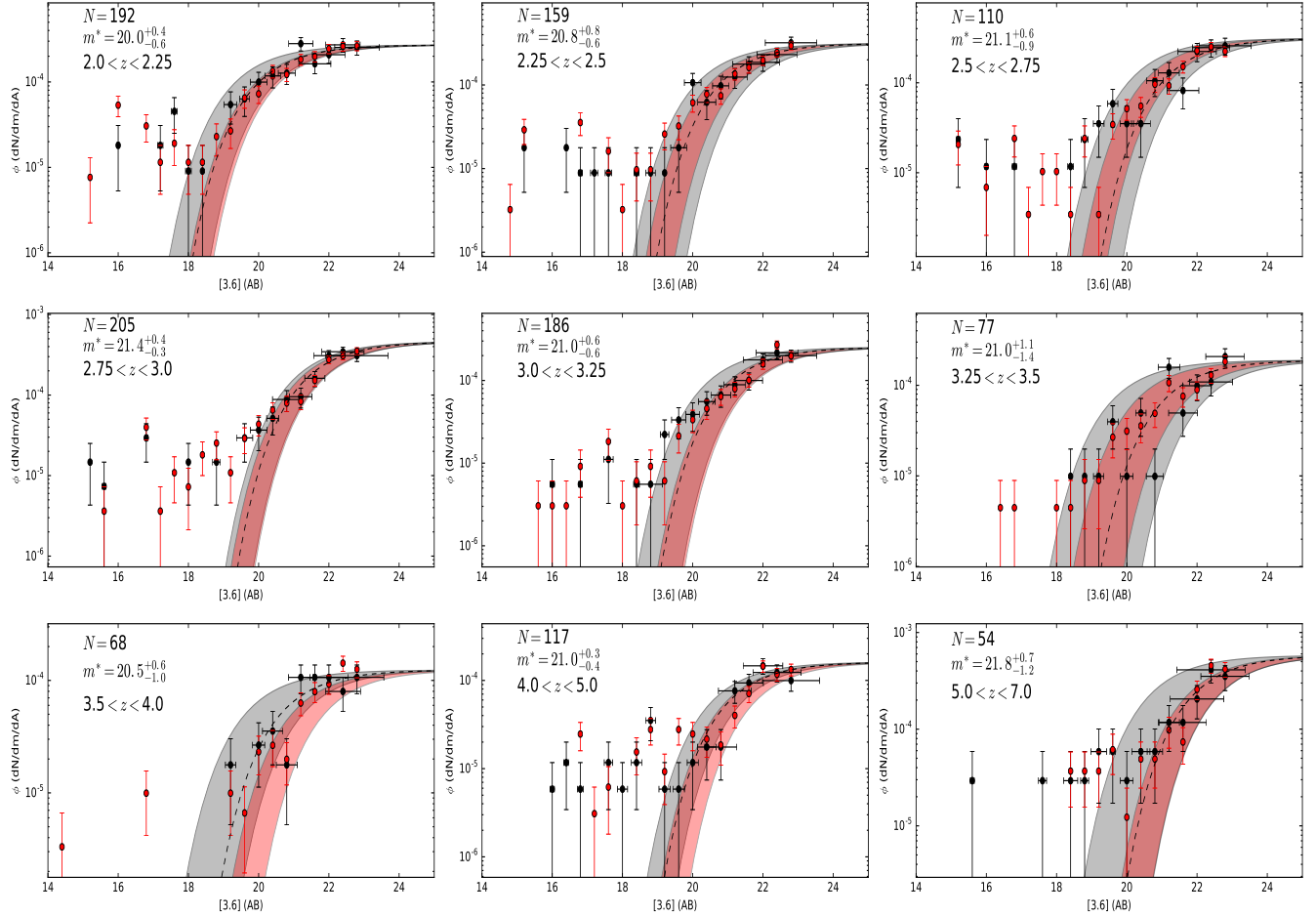


Figure 4. Superimposed on the LF of CCPC galaxies (Fig 2) are spectroscopic ‘field’ galaxies (red points), taken from the same redshift source catalogs and fields as the CCPC candidates (see Appendix). These are simply scaled to the CCPC ϕ values by their relative numbers at each redshift bin ($\phi_{\text{field}}(z) = (N_{\text{CCPC}}/N_{\text{field}})\phi_{\text{CCPC}}(z)$). Within the uncertainties, these distributions show no statistically significant difference. The red shaded regions are the bootstrapped 95% confidence interval for the field galaxies, and they overlap the CCPC’s 2 σ range (gray shaded region) at all times.

2003; Kroupa 2002) and dust extinction (Charlot & Fall 2000). Plotted on the models are the $F160W - [4.5]$ colors as a function of redshift for the CCPC. We only show galaxies with photometric uncertainties in an individual filter of $\sigma < 0.75$ mags. There is no clear preference for a single galaxy type, with a large scatter of blue and red galaxies throughout. We also cannot ascertain a preferred stellar population, dust content or formation redshift from these colors alone for an individual galaxy, as the uncertainties can be too large. For many systems the difference between a star forming galaxy and a passively evolving SSP can be assigned within the errors.

Noiro et al. (2016) spectroscopically targeted two candidate structures identified by Wylezalek et al. (2014) at $z \sim 2$. Their *Hubble Space Telescope* photometry of the overdensity revealed a wide spread of $F140W - [3.6]$ colors of roughly $-1 < F140W - [3.6] < 3$, with a much smaller range for the galaxies with confirmed redshifts (approximately $0.5 < F140W - [3.6] < 2$).

The 3D-HST data (Skelton et al. 2014) coincident with CCPC galaxies in the CANDELS fields at $2.0 < z < 2.05$ has a mean color of $\langle F140W - [3.6] \rangle = 0.5 \pm 0.6$, and a range $-0.4 < F140W - [3.6] < 2.3$. The color range is more broad than the spectroscopic sample of Noiro

et al. (2016), but does not go beyond the full range of candidate galaxies in their protoclusters. This suggests a general agreement of their protocluster galaxy population and ours. Higher redshift CCPC galaxies show little color evolution in this plane as well.

3.4. SED Fitting and Galaxy Stellar Mass

The usual methodology of obtaining stellar masses for galaxies at high redshift is to match a stellar population model with a number of observed magnitudes across a range of filters (e.g. spectral energy distribution (SED) fitting; Magdis et al. 2010). Thus, a galaxy is matched with the stellar age, star formation history, metallicity, initial mass function, and dust content of a given model. Hereafter we will refer to this as ‘traditional’ SED fitting. The implied stellar mass-to-light ratio of the best fit model is then used to compute the M_* of the galaxy. There are a number of degeneracies that arise from this method. This can be particularly important with limited wavelength coverage and inconsistent rest-frame colors over a large range in redshift. These factors will be briefly considered in Section 4.

To test the relative strength of a fit to different model SEDs, we follow the procedure used in Bolzonella et al.

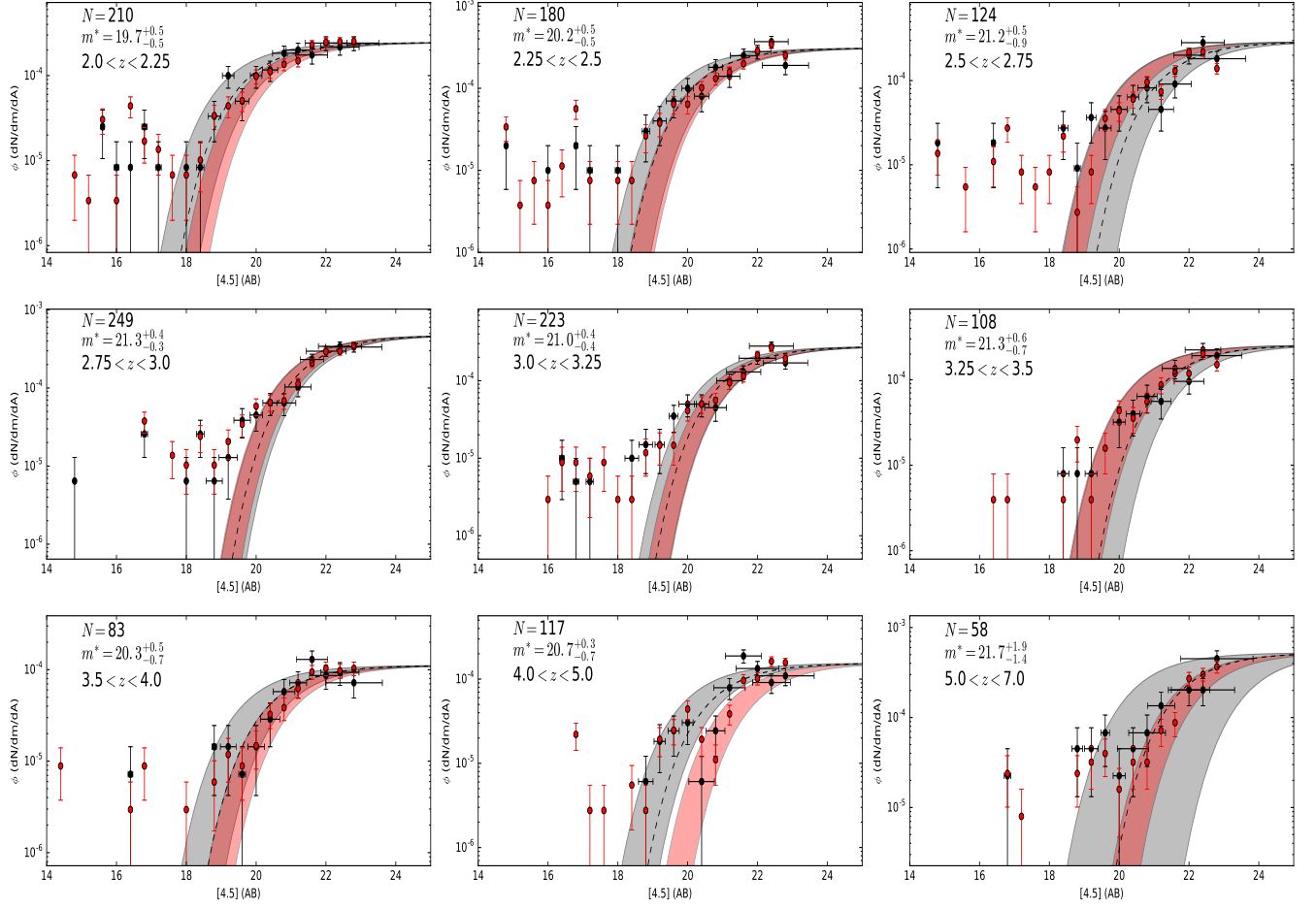


Figure 5. The same as Fig 4 but with [4.5] magnitudes.

(2000) to estimate photometric redshifts:

$$\chi^2 = \sum_{i=1}^{N_{filt}} \frac{(F_{i,obs} - F_{i,model})^2}{\sigma_i^2} \quad (3)$$

which measures the observed flux in a filter ($F_{i,obs}$) relative to the flux of a model stellar population ($F_{i,model}$) and weighted by the squared observational flux uncertainty (σ_i^2). The SED's flux is calibrated to match the observed [4.5] magnitude of the galaxy being measured in our algorithm. We limit our analysis to magnitudes with uncertainties $\sigma_m < 0.75$ and require a F160W measurement. As stated previously, *Spitzer* colors cannot differentiate between varying stellar populations at these redshifts. This maximum allowable uncertainty is effective in limiting severely anomalous photometric measurements from a heterogeneous sample of surveys which do not have a constant depth. We will show that the photometric uncertainties are generally of minor importance when compared to the model degeneracies of our fits. The stellar mass implied by different models for the same redshift and magnitude have greater variance than the uncertainty introduced by photometric errors. This will be discussed further in Section 4.

Using the EzGal code (Mancone & Gonzalez 2012), we built grids for each filter and stellar population model as a function of formation redshift ($2 < z_f < 10$) and ob-

served redshift (z_{obs}). We consider the following models: BaSTI simple stellar populations (SSPs) with metallicities of $Z = 0.008, 0.0198$ (Percival et al. 2009) and a Kroupa IMF (Kroupa 2002), Bruzual & Charlot (2003) (hereafter BC03) constant star formation models with extinctions of $\tau_V = 0.2, 1.0$ and a Chabrier (2003) IMF, and two BC03 exponential decaying SF models with $\tau = 1.0$ Gyrs and $Z = 0.008, 0.02$. The model predictions become erratic when the stellar age of the system is low, so we implemented a cut of $z_f - z_{obs} > 0.05$ when fitting the formation redshift.

For the models that did not have a dust component built in, we also explicitly calculated the extinction from a Charlot & Fall (2000) model for the rest-frame wavelengths observed in our filters at a stellar age computed from the z_f value in the grid. The dusty fluxes were re-computed and the fits measured using Equation 3 in the same manner as the dust-free systems.

Once the best-fitting model is identified for each galaxy, we calibrate the model to the observed magnitude m_i , for each filter measured (i), and query EzGal for the implied stellar mass at the observed redshift. For an individual filter's mass measurement, $M_{i,*}$, we estimate its uncertainty by taking the implied mass of the galaxy if the magnitude was changed by its photometric uncertainty ($m_i \pm \sigma_i$) in that filter. Ultimately, the estimated stellar mass of the system is computed from the uncertainty-weighted mean value from each wavelength

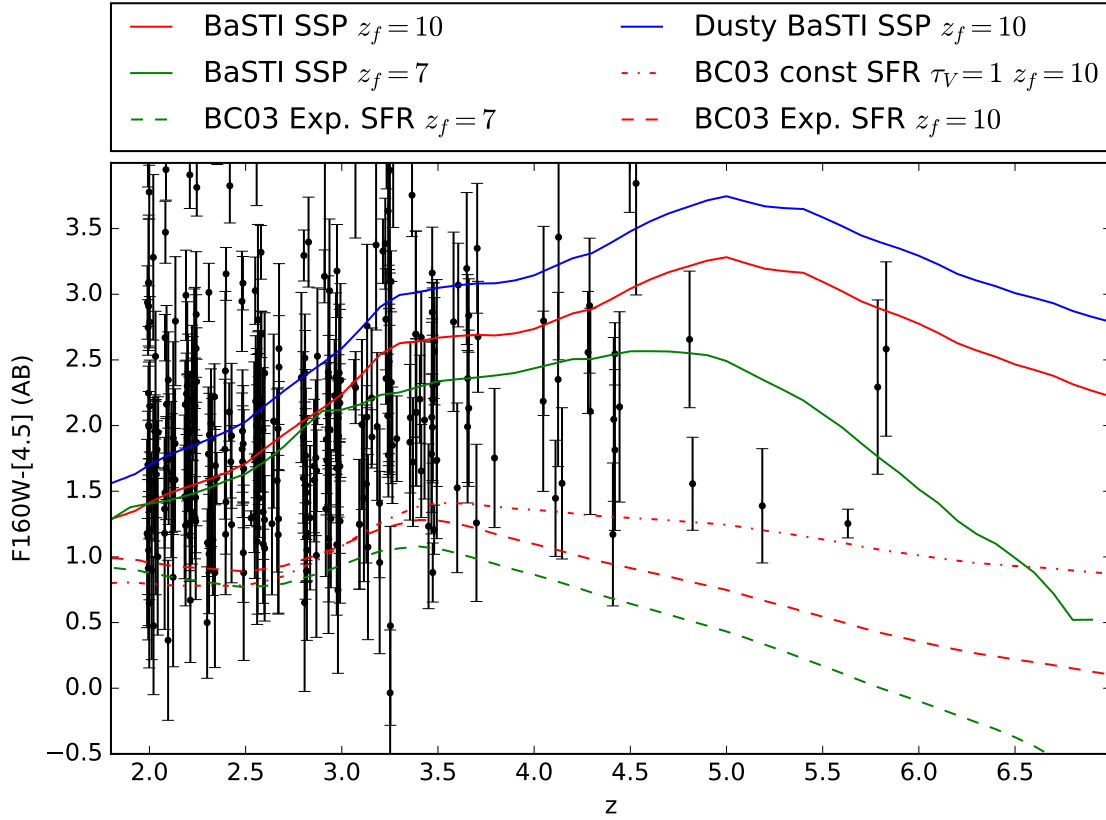


Figure 6. We plot the $F160W - [4.5]$ color evolution of six stellar populations: two BaSTI SSPs at $z_f = 7, 10$ (green and red solid lines, respectively), with an added [Charlot & Fall \(2000\)](#) dust component to the $z_f = 10$ SSP (blue solid line), along with two BC03 exponential decaying SFR with $\tau = 1$ Gyr at $z_f = 7, 10$ (green and red dashed lines), and finally a constant star formation model with an extinction of τ_V and $z_f = 10$ (red dot-dashed line). All models have solar metallicity. Plotted as black points are the colors of CCPC galaxies. These span the entire range of model stellar populations. For an individual galaxy, the uncertainties are generally too large to be assigned to one model or another. However, most systems can be separated between SSPs (generally quiescent) and star forming models.

measured. If the system is found to have a best-fit SED that is dusty, we subtract the dust absorption from the observed magnitudes prior to computing the underlying stellar mass estimates.

In this manner, we were able to fit 414 galaxies that were below a minimum χ^2 threshold, with a median value of $\chi^2 = 1.6$ and a median of $N_{\text{filters}} = 3$ ($F160W$, $[3.6]$, and $[4.5]$). Fig 7 shows a few examples of SED fits with a variety of χ^2 values. The median mass implied for these galaxies is $3.3 \times 10^{10} M_\odot$. Nearly half of the systems were best fit by an exponentially decaying, BC03 star forming model (185 objects), with 201 others well fit by a BaSTI simple stellar population. Roughly 50% of galaxies were found to be best fit by a dusty component, and only 18% had less than solar metallicity. The average formation redshift fit by the algorithm was generally old, at $z_f = 7.9$. The 3D-HST data ([Skelton et al. 2014](#)) has greater wavelength coverage in *Hubble Space Telescope* filters within the CANDELS fields. The fits to 395 SEDs using this expanded data set did have a marginally smaller median M_\star value of $0.9 \times 10^{10} M_\odot$, a lower percentage of dusty galaxies (27%), and 51% low-metallicity systems (compared to $< 15\%$ in our data set). The 3D-HST catalog’s photometry did not use aperture corrections in their *Spitzer* magnitudes, which (if instituted) would systematically increase the stellar mass of these galaxies. Only 7% of the 3D-HST galaxies were

best fit by a BaSTI SSP, while the BC03 constant star formation models was applied to roughly 1/3 of CCPC sources. The majority were fit by an exponential model, just like our own photometric set. The mean formation redshift for the 3D-HST photometry was $z_f = 5.9$. The 3D-HST fits have a median value of $\chi^2 = 30.5$.

With the recent success of modeling galaxy SFHs as a log-normal distribution ([Gladders et al. 2013](#); [Abramson et al. 2016](#)), we attempted to fit the CCPC with a similar analysis. The log-normal distribution adopted is of the form

$$SFR \propto \frac{\exp\left(-\frac{(\ln(t)-T_0)^2}{2\tau^2}\right)}{t} \quad (4)$$

where t is the time since the Big Bang, T_0 is the half-mass time of the galaxy, and τ is the half-mass width of the distribution ([Abramson et al. 2016](#)). We took the two BaSTI SSPs (different metallicities) as our base models, and then computed Complex Stellar Populations (CSPs) using EzGal for a variety of values of T_0, τ ranging from $0.05 \leq (T_0, \tau) \leq 1.0$. This range corresponds to the breadth of values fit to observed SEDs at low and high redshifts ([Gladders et al. 2013](#)). We evaluated the goodness-of-fit with Equation 3, as before. We included the optional [Charlot & Fall \(2000\)](#) dust extinction by assuming a stellar population age (z_f) coincident with a

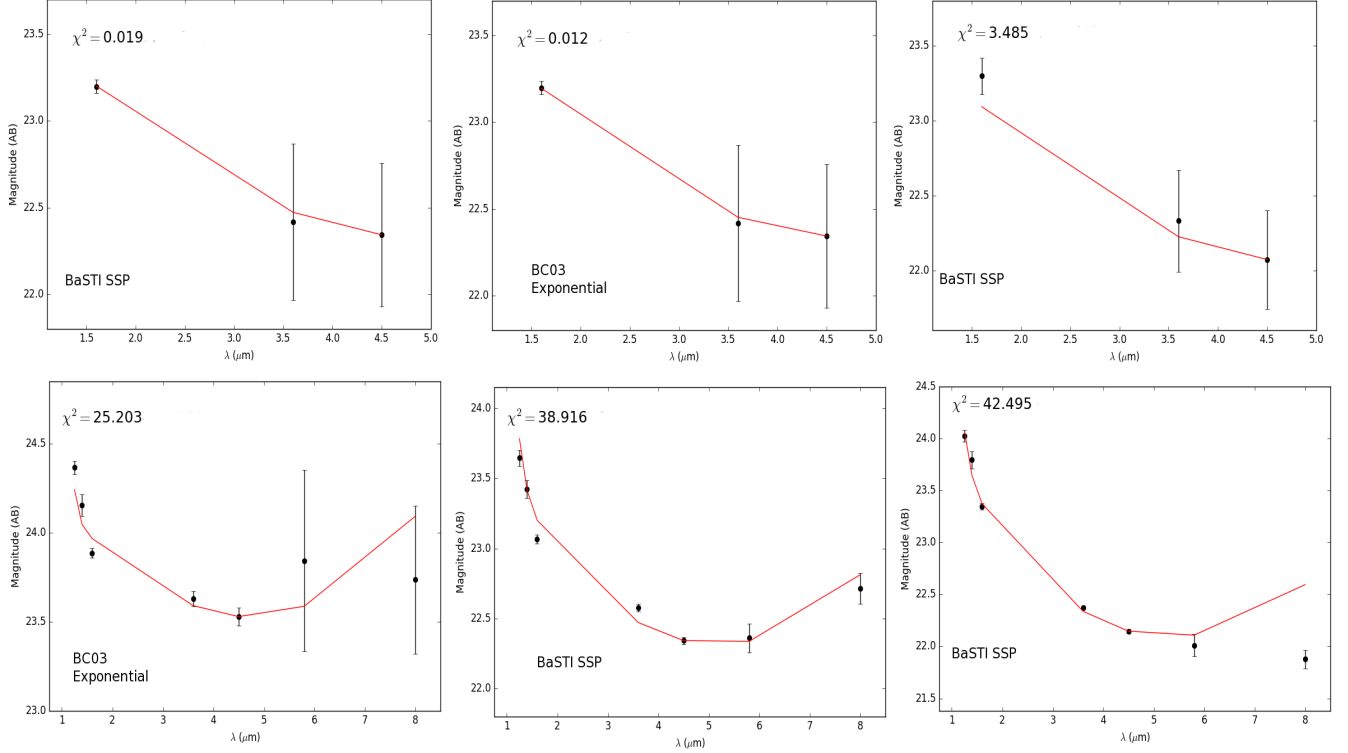


Figure 7. *Top:* Three examples of CCPC galaxy SED fits. The black points are the apparent magnitudes at observed wavelengths (F160W, [3.6], and [4.5] filters), while the red lines are the template magnitudes. The formation redshifts, from left to right, are $z_f = 3.0$, 7.0, and 3.25. The left and right templates are BaSTI SSPs with solar metallicities, while the center template is a BC03, exponentially decaying model with $\tau = 1$ Gyr. The χ^2 values of the fits are listed, which are used to distinguish the relative goodness-of-fit between various models for a single galaxy. *Bottom:* CCPC galaxies found within the 3D-HST database (Skelton et al. 2014) can have greater wavelength coverage (F125W, F140W, F160W, [3.6], [4.5], [5.6], and [8.0]), although these are limited to the GOODS fields. The templates presented are dust-free. The left panel is a BC03 exponential model with $\tau = 1$ Gyr and metallicity of $Z = 0.008$, while the middle and right panels are BaSTI SSP with solar metallicities. They have $z_f = 3.75$, 3.0, and 3.5 from left to right, respectively. The larger χ^2 values of the models in this panel compared to the Top panel are the result of more measurements (with relatively small uncertainties) from which a galaxy model can differ. They are not necessarily a poorer fit. The χ^2 values also depend upon the inherent biases within the models as well, and should therefore not be treated as an absolute metric.

$\text{SFR}(t) = 10^{-3}(\text{SFR}_{\text{max}})$. The factor 10^{-3} is fairly arbitrary, with an order of magnitude adjustment changing z_f by approximately 0.2.

The log-normal routine was able to adequately describe only 207 galaxies, roughly half of the traditional number of successful SED fits. The fits were also poorer than the traditional fitting, with a median $\chi^2 = 24.6$ (compared to $\chi^2 = 1.6$). This is somewhat surprising, as the volume of parameter space explored was much larger than in traditional fitting. The median mass for these galaxies ($1.5 \times 10^{10} M_\odot$) was similar to the traditional fit, with no preference for low metallicity systems (15%). Nearly 85% of the galaxies were best fit with a dust component included. The mean formation redshift was $z_f = 10.7$, only slightly older than the stellar age from traditional fitting. The median values of T_0, τ are 0.05 and 0.15 (~ 1.05 and 1.16 Gyrs), respectively. Running the SED fitter on the 3D-HST data set generally confirms the earlier results from our photometry, with a few notable exceptions. Interestingly, more galaxies were successfully fit by using the larger wavelength coverage (262) but with a much lower fraction of dusty systems (0.33), a larger mean T_0 (0.65), an older mean stellar population ($z_f = 14.6$), and a slightly lower median mass than the traditional models ($0.7 \times 10^{10} M_\odot$). The median values of $\tau = 0.15$ was equivalent to the log-normal value de-

rived with our photometry. The 3D-HST fits had a similar value of $\chi^2 = 21.7$ to the log-normal fit of our data, but are in fact more robust, as more filters were used. We will also briefly note that although the median values here may appear to be slightly different if traditional or log-normal SED fitting is used, or the 3D-HST data adopted versus our own photometry, the variance of the properties are much larger than their differences. This suggests that the underlying properties of these galaxies are still very uncertain. This will be discussed further in Section 4.

Many galaxies have no *Hubble Space Telescope* photometry in the CCPC. In order to estimate their M_* we adopt the simple BC03 exponential decaying SF model with a metallicity of $Z = 0.02$, $\tau = 1$ Gyr, and $z_f = z + 0.25$. This choice is reasonably justified, as the majority of the CCPC galaxy sample was selected as unobscured star forming systems (UV-bright LBGs or $\text{Ly}\alpha/\text{H}\alpha$ line-emitters), and this exponential model appears to be a consistent fit with the evolution of m^* . It supplies a conservatively low mass estimate for the system.

Figure 8 plots the galaxy stellar masses of the objects measured by various SED fitting methods. The scatter is large, even for a single galaxy fit by different algorithms (log-normal versus traditional) or different pho-

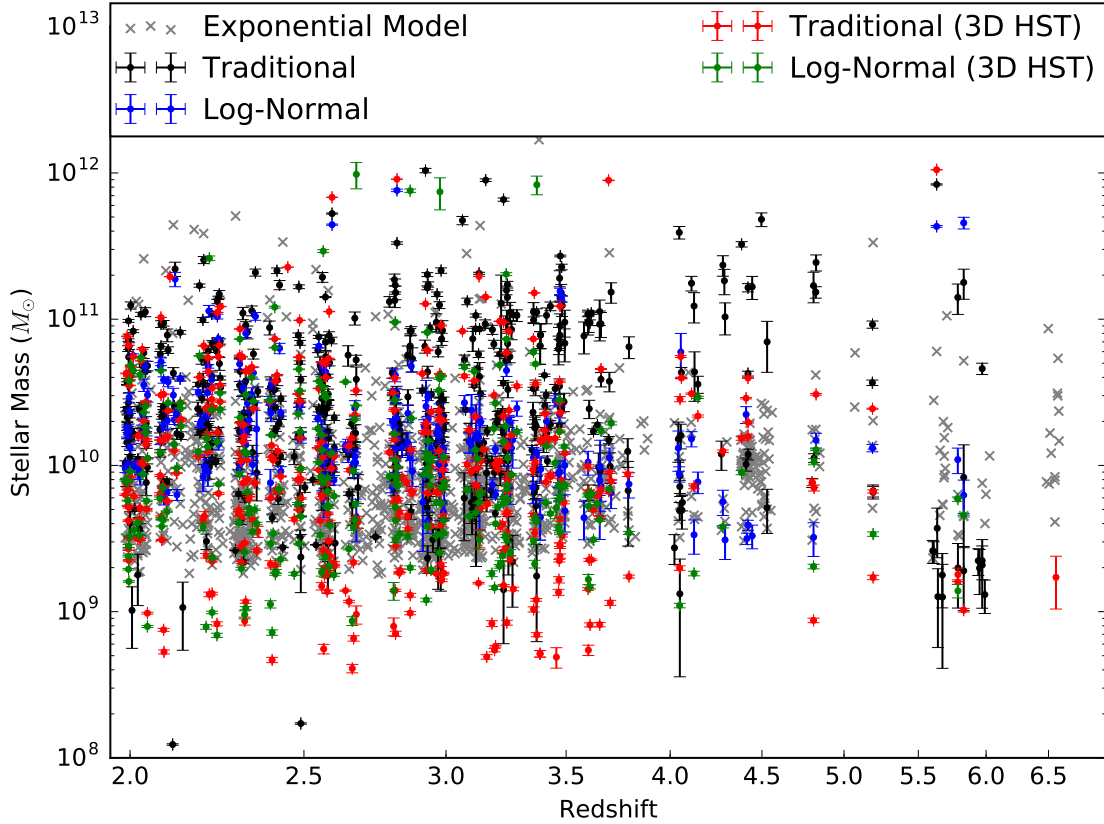


Figure 8. The stellar masses (in units of M_{\odot}) as a function of redshift (note the logarithmic scale) for CCPC galaxies estimated via traditional SED fitting (black points), and log-normal SFH fitting (blue points). All galaxies with a $[4.5]$ measurement are shown as gray points, which assume a young, bright stellar population with an exponentially decaying SFR. Also included are galaxies photometrically measured by the 3D-HST project (Skelton et al. 2014) by traditional and log-normal SED fitting (red and green points, respectively). Individual galaxies with more than one stellar mass estimate can have large variances (much larger than the photometric errors) based on the model selected with the minimum χ^2 value. For instance, a bright galaxy with a young stellar population can have an order of magnitude lower stellar mass than the same galaxy fit by an old SSP. We are not able to adequately select a unique model for a given galaxy with our data. The masses are the uncertainty-weighted mean values from the adopted population model. The gray error bars are suppressed for clarity, but are generally larger than the other data points, as they are only measured at $4.5\mu\text{m}$. The galaxies with the largest stellar masses are typically the ‘hyperluminous’ sources seen in in Figs 2 and 3, as expected. These include a probable mix of AGN, low-redshift interlopers, and simply massive systems.

tometry (3D-HST versus our own). The gray points are the conservative mass estimate for each galaxy, which is simply an exponential model (BC03, $Z = 0.02$, and $z_f = z + 0.25$ described above). These points can be thought of as lower limits of stellar mass for individual galaxies. An example presented in Section 4 will illustrate the circumstances in which this is the case.

4. DISCUSSION

4.1. Hyperluminous Sources

It is clear that the Schechter function fits the data adequately within a few magnitudes around m^* . However, there are some very bright sources ($m \leq m^* - 2$) that are clearly anomalous in Figures 2 and 3. These points are rare, generally consisting of 1-3 galaxies per bin, but they are apparent at all redshifts and at both wavelengths. In the context of Λ CDM and hierarchical accretion, it is predicted that in the densest regions of the universe at high redshift ($z > 2$), the most massive galaxies will reside (Muldrew et al. 2015). Therefore, protocluster galaxies might be expected to be in the most massive halo systems. Curiously, field galaxies appear to have the same proportion of hyperluminous galaxies as their overdense

counterparts (Figs 4, 5). We will discuss a few other possibilities for the origin of these sources.

In their Fig 23, Guo et al. (2011) plot their semi-analytic model (SAM) Schechter stellar mass functions at redshifts $2 < z < 4$, overplotted with observational data from Pérez-González et al. (2008) and Marchesini et al. (2009). The data diverge from those models in much the same manner as the data presented here, with a number of bright objects not fit by the exponentially declining number density. At a redshift of $z \approx 7$, Bowler et al. (2014) find a similar trend at rest-frame UV wavelengths. It could be possible that at these epochs, Eq 2 is not representative of the stellar mass of galaxies. There is some indication that the most massive galaxies observed at very high redshifts ($z > 4$) had not the time to assemble in a Λ CDM universe (Steinhardt et al. 2016), and their halo mass density is larger than theoretical predictions. Some of the hyperluminous sources may be these galaxies and their descendants.

AGN can have strong, non-stellar emission that dominates the flux of the galaxy. These objects are contributing to the number of hyperluminous sources. Roughly half of the hyperluminous objects were spectroscopically

selected as part of quasar and AGN surveys, and additionally some of our data come from targeted overdensities surrounding these types of sources, as in [Venemans et al. \(2007\)](#). There is also some evidence that AGN are found in greater density surrounding protoclusters ([Casey et al. 2015](#)). However, AGN are quite rare in LBG studies ([Magdis et al. 2010](#)).

Some of these objects were detected using NB filters centered on redshifted $H\alpha$ or $Ly\alpha$ lines, which were then confirmed to be emission lines spectroscopically. However, emission line galaxies can be incredibly faint and show little or no continuum emission ([Fynbo et al. 2003a](#)), and thus no other absorption or other emission features are identified. Therefore, some of these objects could be [O II] emitters ($\lambda\lambda 3726, 3729$), or other line-emitting galaxies at lower redshifts, and are therefore less distant than expected. [Venemans et al. \(2007\)](#) discuss various tests than can be used to disqualify candidate $Ly\alpha$ systems, and they estimate that interlopers are $\leq 10\%$ in their sample. These low redshift interlopers could account for a few of these hyperluminous sources.

4.2. Field Galaxy Comparisons

More massive galaxy halos are systematically found in denser environments. This is an observed effect at high redshift, where the two-point correlation function amplitude appears tied to the UV luminosity of LBGs ([Ouchi et al. 2004b](#)). It also has a theoretical basis found within large Λ CDM simulations, where the most massive galaxies reside almost exclusively in the densest environments ([Muldrew et al. 2015](#)). However, it is readily apparent in Figs 4, 5 that the luminosity functions of field galaxies are in no way distinct from their CCPC galaxy counterparts. They contain an equal measure of hyperluminous sources, and their respective Schechter function parameters are equivalent.

Taken at face value, the rest-frame NIR emission of galaxies at all redshifts and densities are essentially equal, and therefore their stellar mass contents should be similar as well. In order to reconcile this fact with the points laid out in the previous paragraph, we will suggest a few possible solutions. We note that our data are not sufficient to endorse any of these over another. The null hypothesis is that the galaxy stellar populations at $z > 2$ are the same, regardless of environment.

If galaxies in protoclusters are inherently brighter, as expected, but also had a greater fraction of dusty galaxies or more dust extinction in general, this could balance the magnitude of field and protocluster galaxies. Assuming a [Charlot & Fall \(2000\)](#) dust model, we can predict the dust extinction for a given wavelength and stellar age. At the redshifts measured, it is a low extinction of median $\Delta m \sim 0.6$ mags for a starbursting galaxy and $\Delta m \sim 0.3$ mag for an older population from $2 < z < 4$ at $4.5\mu\text{m}$, with the extinction increasing at higher redshifts. This hypothesis would require an extremely convenient steady increase in dust absorption across the range of rest-frame emission to account for the stellar mass difference between protocluster galaxies and the field. The maximum extinction during a starburst is hardly significant ($\Delta m \approx 0.6$ mags), and might not be detected within the uncertainties of m^* .

Another option is that our selection of ‘field’ sources actually targets marginally overdense systems, and are

therefore not isolated enough to be different from the CCPC systems. As a reminder, the initial ‘Field’ sample was composed of galaxies within the same survey fields as the CCPC galaxies to minimize bias, but were not found within the same volume as a CCPC candidate. After this sample showed no differentiation, a smaller subsample was crafted which contained $N < 4$ galaxies in the same volume as the CCPC. This also did not show any difference in the LFs when compared to the CCPC. Analysis of galaxies limited to the GOODS-S survey also showed no statistically distinct difference, suggesting that in this particular instance, the myriad of spectroscopic selection functions of the CCPC galaxies did not dilute a potential signal.

[Contini et al. \(2015\)](#) analyzed zoomed-in protocluster galaxies in a SAM, and found that for galaxies in the region of a protocluster, but not bound to it at $z = 0$, the galaxy properties (color, mass, etc.) were indistinguishable. It is possible these field galaxies may be similarly camouflaged. A related plausibility is that a large number of interlopers within the overdensity volumes mask a detectable differentiation. If, however, the rarest, most massive galaxies form only in the densest regions of the universe ([Muldrew et al. 2015](#)), then presumably some evidence of these could be solely evident in the CCPC LFs. Recently, [Hatch et al. \(2016\)](#) found evidence suggesting that dense sub-groups in a protocluster at $z \sim 1.6$ exhibited differentiation with respect to the field, while 2/3 of the member galaxies outside of groups showed no variation.

A further possible, but poor, explanation is that the spectroscopic selection of the surveys used are more incomplete in these field regions than in the CCPC volumes, and therefore may well be overdense themselves. However, spectroscopic completeness is strongly correlated to flux for practical purposes, and we see no difference with galaxy densities brighter than m^* . At the present time, we do not have a satisfactory explanation for this discrepancy.

4.3. m^* Evolution

In the context of previous works, our results for the redshift dependence of m^* are puzzling. [Mancone et al. \(2010\)](#) and [Brodwin et al. \(2013\)](#) analyzed the *Spitzer* LFs and SFR (respectively) of the same cluster sample at $z < 2$. They conclude that the epoch at which cluster galaxies are undergoing rapid mergers (and therefore mass assembly) is approximately $z \sim 1.5$. [Wylezalek et al. \(2014\)](#) investigated the *Spitzer* LF of clusters and protoclusters at $z \leq 3$, and find no evidence of such a rapid mass assembly at $z \sim 1.5$. They find that a passively evolving stellar population is consistent with the full $m^*(z)$ range of both [Mancone et al. \(2010\)](#) and [Wylezalek et al. \(2014\)](#). [Wylezalek et al. \(2014\)](#) hypothesize that as they are probing higher redshifts, and thus rarer/denser volumes, they do not observe the mass assembly seen at $z \sim 1.5$ by [Mancone et al. \(2010\)](#), which correspond to more common overdensities. As a result, they speculate that it might be possible to observe a different epoch of cluster assembly at higher redshifts ($z > 3$) than their sample. This is akin to a cluster-scale version of galaxy downsizing, where the densest clusters will form the quickest. We do not see any behavior analogous to the high redshift ($1.5 < z < 2.0$) m^* variability

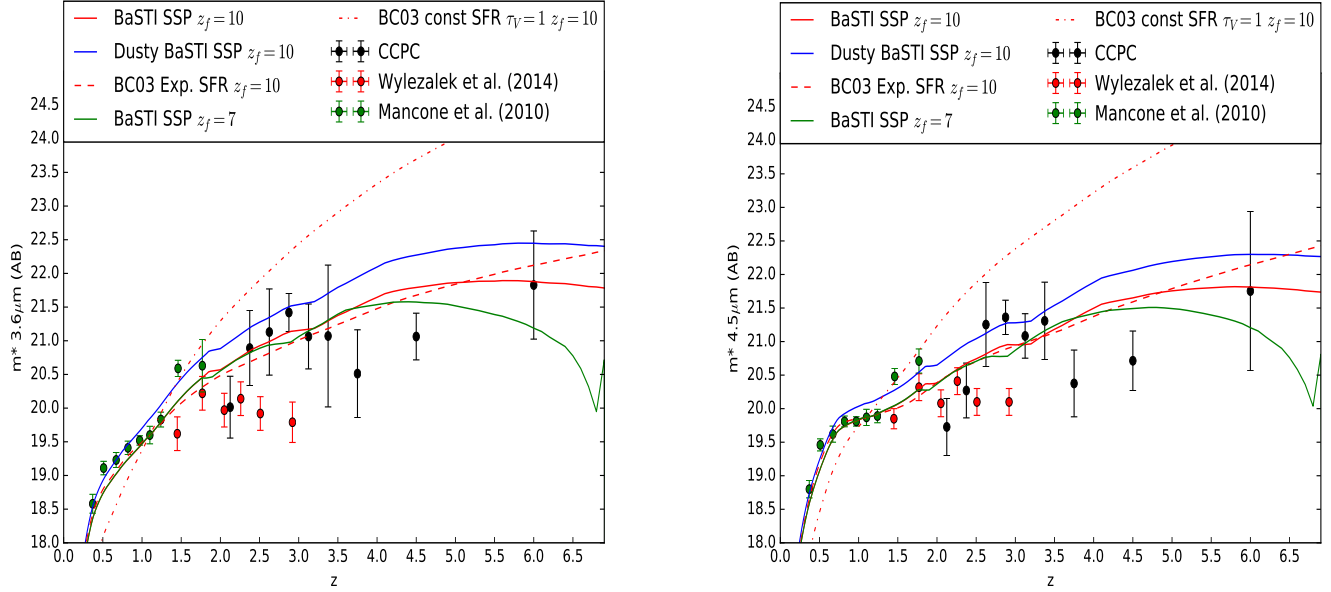


Figure 9. We show the evolution of m^* as a function of redshift for $3.6\mu\text{m}$ (Left) and $4.5\mu\text{m}$ (Right Panel). The black points are the CCPC values, while green and red values are from Mancone et al. (2010) and Wylezalek et al. (2014), respectively. The error bars shown for the CCPC are 1σ values computed by bootstrapping. Overplotted are various models computed using EzGal. Briefly, we have included two BaSTI simple stellar populations at formation redshifts $z_f = 7, 10$ (solid green and red lines, respectively), and added a Charlot & Fall (2000) dust prescription to the $z_f = 10$ SSP (blue solid line). From the BC03 models, we included an exponentially declining SFR model with $\tau = 1$ Gyr (dashed red line) and a constant star forming model with an extinction of $\tau_V = 1$ (dash-dot red line). This latter model provides a poor fit to the m^* evolution, while the two SSPs ($z_f = 7, 10$) and exponential model are consistent with the data. Each model is scaled to match the $z = 1.1$ m^* value from Mancone et al. (2010), although this choice is not unique. The scaling simply moves the evolution curves to brighter or fainter magnitudes, but the shape remains constant. Therefore, for any scaling choice, a constant star forming model will provide a poor fit. The dust model was originally calibrated to the same m^* value as the others, but was not re-scaled to show the effect.

of Mancone et al. (2010) in our sample, which would indicate rapid mass assembly.

When our data is analyzed with the two previous works (Fig 9), the evolution of the characteristic magnitude (m^*) is fully consistent with a simple stellar population formed at $z_f \leq 10$. Even more puzzling is that the field sample at these redshifts is equivalent in all respects to the overdense sample, apart from the scaling. We gain little insight into the epoch of rapid mass assembly of cluster galaxies, or of the field for that matter. More complex stellar populations, such as an exponential decay model with $\tau \sim 1$ Gyr, can also be consistent with the data. A constant star formation model is not favored, regardless of which $m^*(z)$ value it is calibrated to.

It should be noted that this is not a progenitor-matched study, in that as the redshift increases, the possibility of detecting a weak overdensity will decrease. CCPC candidates at $z > 4$ will likely not evolve into the $z = 2$ candidates from Wylezalek et al. (2014) in a one-to-one fashion. However, some overlap could occur, particularly with their strongest overdensities. From our simple analysis, it appears that *Spitzer* m^* values in dense environments, a tracer of the stellar mass content of these galaxies, is consistent with the passive evolution of a single burst of star formation at $z_f = 10$ over nearly 10 Gyrs ($0.3 < z < 6.6$) of time.

It could be hypothesized that the marginally overdense CCPC candidates could merely be field galaxies. Their inclusion in the luminosity functions (Fig 4 and Fig 5) could thus mask a weak signal of differentiation in the stellar mass functions of protocluster versus field galax-

ies. As a simple test of this hypothesis, we re-computed the $[4.5]$ m^* values for sub-samples of galaxies that exist in overdensities of $\delta_{gal} > 2, 3, 4$ and 5. The redshift and magnitude bins remained unchanged from the analysis of the total sample. The m^* redshift evolution of these sub-samples are broadly consistent with the 2σ uncertainties presented Table 2. There appears to be no statistically significant correlation between m^* and δ_{gal} within our limited sub-samples. For CCPC galaxies at $z < 3.25$, m^* is brighter by less than 0.3 mags between the sub-samples of $\delta_{gal} > 4$ and $\delta_{gal} > 2$, on average. This is consistent with the uncertainties listed in Table 2. Significant deviations between the total and sub-samples of $\Delta m^* > 1$ occur only in some high redshift, high overdensity bins that lack significant galaxy numbers ($N \sim 10^1$) to provide a satisfactory solution.

4.4. Galaxy Selection Implications

A further curiosity is evident when the evolution of m^* is considered in the context of the galaxy type predominantly represented in our sample. CCPC galaxies generally originate from LBG and line-emitting galaxy (*Lya* emitters) spectroscopic surveys, which are selected directly because of their large UV-luminosity/SFR. Fig 9 illustrates that a consistent fit to the model of m^* galaxies from $0.3 < z < 6.6$ is a simple stellar population, not a constant star formation model, dusty or otherwise. At low redshifts this is not surprising, as a passive stellar population model has historically been well fit to overdense regions (Stanford et al. 1995). However, the high redshift systems are star forming galaxies *by selection*,

and yet the data clearly disfavor the model. The exponential decaying SFR model (Tinsley 1972) with $\tau = 1$ Gyr is also consistent with the evolution of m^* . However, this type of model is not able to fit roughly 1/4 of all $z = 0$ galaxy SFHs (Oemler et al. 2013). Exponential decay models with $\tau = 10$ Gyrs look similar to that of the constant star formation model. Fig 9 is normalized to match the data of Mancone et al. (2010) at redshift $z < 1.1$.

It could be assumed that by normalizing the star formation model to a different $m^*(z)$ value, the data might be better fit. However, the shape of the model does not change, just its scaling. The constant SFR model will be too bright at lower redshifts and too faint at higher redshifts, regardless of the scaling. However, this simple observation should not be considered wholly unreasonable. There were a variety of individual sources that were fit with SED templates of exponential decaying SFRs, which are still forming stars at these early epochs of the universe, and the $\tau = 1$ Gyr model in Fig 9 is consistent with the data. At these wavelengths, the predictions between a young, SSP and a decaying SFR cannot be disentangled within the uncertainty of the data.

An important factor to consider in the context of this entire work (not just the m^* evolution) is that our spectroscopic galaxy sample does not consist of the majority of galaxies at $z > 2$. In fact, van Dokkum et al. (2006) showed that approximately 80% of galaxies are not LBGs between $2 < z_{\text{phot}} < 3$. Many of these other objects are distant red and dusty star-forming galaxies (DRGs and DSFGs). This trend appears to become even more pronounced at higher redshifts. In the range of $3 < z < 4$, only 14% of galaxies with photometric redshifts would be identified as LBGs, with the remainder being nearly split between DSFGs and DRGs (Spitler et al. 2014). It is unclear, without spectroscopic confirmation of protocluster membership, how these DRGs/DSFGs might cluster differently than their LBG counterparts, or if they might have LFs that vary with environment.

These DRGs are forming a not-insignificant amount of stars, on the order of a 20% contribution to the cosmic star formation density at $1.5 < z < 2.5$ (Webb et al. 2006). They therefore may not be completely unlike the spectroscopic galaxies in our sample. Unfortunately, Spitler et al. (2014) noted that most of these DRGs are much fainter (~ 2 mags) than the canonical spectroscopic limit of $R_{AB} \leq 25.5$ for current instrumentation. For the present, it appears that this question will remain unanswered in the context of a spectroscopically-confirmed protocluster sample like the CCPC.

Although we do not expect to have DRGs/DSFGs in the CCPC, which are the dominant galaxy populations at high redshift, we can make comparisons to cluster and protocluster candidates that do have these systems at lower redshift. In fact, we have already performed such an analysis, in that Mancone et al. (2010) and Wylezalek et al. (2014) do not rely solely on spectroscopic redshifts for cluster membership. Mancone et al. (2010) compute photometric redshift probabilities from deep, multi-wavelength data, while Wylezalek et al. (2014) utilize *Spitzer* color cuts to identify high redshift galaxies in their overdensities. Both of these techniques are sensitive to galaxy populations not characterized by bright UV continuum selection (e.g. LBGs). As the entirety of

the m^* evolution is consistent with a simple stellar population, passively evolving, it is plausible that the LFs of DRGs and spectroscopically confirmed LBGs may not be significantly divergent at these redshifts. Indeed, the redshifts at which Wylezalek et al. (2014) and this work overlap are in agreement within the uncertainties, despite the differences in selection.

4.5. Inferred Stellar Masses and Galaxy Properties

SED fitting is an incredibly useful tool for estimating redshifts and galaxy properties at high redshift over a range of populations (Bolzonella et al. 2000; van Dokkum et al. 2006). However, it is possible to fit more models and parameters to the data than can actually be constrained. In addition, there are significant degeneracies among model parameters that can match the same data at these high redshifts (Papovich et al. 2001a; Magdis et al. 2010), such as the well known age-metallicity-dust degeneracy. The models differ among themselves, with varying treatment of thermally-pulsating asymptotic giant branch stars or the adoption of varying IMFs (Bruzual & Charlot 2003; Percival et al. 2009). Furthermore, with little *a priori* knowledge of the uncertain galaxy zoo extant at high redshift, the difficulties compound. These issues are indeed true in the case of the CCPC, with our limited wavelength coverage, as well as in numerous other studies. However, some properties can be loosely constrained by our data, and is therefore a useful exercise if one is cognizant of the limitations of SED fitting.

Primarily, the rest-frame NIR data provided by *Spitzer* provides a proxy for the underlying stellar mass of the CCPC galaxies at high redshift. Unfortunately, for the same reason they are a powerful tool for measuring stellar mass, these colors provide little information in determining any other property of the underlying galaxy (e.g. passive versus star forming, metallicity variations, formation redshift; see Cooke et al. 2014). *Hubble Space Telescope* filters (e.g. F125W, F140W, F160W) that measure rest-frame optical bands at the redshifts of the CCPC are able to generally distinguish between passive and star-forming galaxies. In Fig 6, a number of model stellar populations are plotted as a function of redshift and F160W-[4.5] color. A clear bifurcation is shown at $z \sim 2$ which grows more pronounced at larger redshifts. Within the photometric errors of our colors, it is not possible to assign a preferred star formation rate or formation redshift to the CCPC galaxies. Clearly a range of stellar populations may exist. Dust obscuration is also uncertain, as a typical reddening of these colors is ~ 0.5 mags or less for the BaSTI SSPs. This which is the 1σ photometric uncertainty in many cases.

To briefly illustrate the perils of mass estimation among various models, let us take an idealized example of a galaxy with a measured $[4.5] = 20$ AB magnitude. We can infer the stellar mass of this system from a menagerie of models available using a formation redshift $z_f = 10$ and solar metallicity. At $z = 2$, the observed system can have a range of $1 \times 10^{11} < M_* < 3 \times 10^{11} M_\odot$ for the extreme cases of a BC03 SFG to a BaSTI SSP, respectively. At a redshift $z = 6$, this gap can widen to roughly $4.5 \times 10^{11} < M_* < 9.5 \times 10^{11} M_\odot$. Lowering the formation redshift will also decrease the implied stellar mass by a factor of ≤ 3 . Notice that this example did not take into

account any photometric uncertainties, dust, metallicity variations, or flux measurements at other wavelengths. A change in z_f can have an outsized role if it is close to the redshift of the galaxy (e.g. a young galaxy). An old, bright galaxy can have $10\times$ the stellar mass than that of a young system of the same luminosity.

In practice, the χ^2 values from successive SED fits were observed to not change significantly. This was in spite of their sometimes drastically different stellar populations (e.g. quiescent versus star forming). A brief examination of Figure 6 reveals that various models can exist within the color uncertainty of the CCPC galaxies. We wish to caution readers that SED fitting can have a difficult time *excluding* models, especially with the limited wavelength coverage presented here. Therefore, stellar mass uncertainties are dominated by systematic variations in the models and the subsequent fitting procedure.

Comparing the model fits on a system-by-system basis provides a cautionary tale for determining galaxy properties (mass, age, metallicity) via the SED fitting method. We applied our algorithm, for both log-normal and more traditional SEDs, to the data we measured, in addition to a companion photometric catalog in the CANDELS fields (3D-HST; Skelton et al. 2014). The stellar mass estimates could vary by an order of magnitude or more for a single galaxy, but we found *no* statistically significant trends among the combination of two data sets and the two SFH prescriptions (log-N versus traditional). Although there might appear to be a mean offset of formation redshift between our data and the 3D-HST catalog of $< z_f - z_f(3D) > \sim 2$, for instance, the scatter between the two ($\sigma = 4.5$) is much larger. The mean mass and χ^2 differences follow much the same pattern, where occasionally a galaxy will be better fit or more massive via log-normal fitting, but a subsequent galaxy will have the opposite effect. This appears to be a classic case of overfitting the data, with various models supporting divergent implications (SFG vs. quiescent) being equal fits to the photometry. It does not appear we are able to constrain the stellar populations or masses for the CCPC galaxies with any reliability.

Despite these concerns, our estimated stellar masses are not wholly unreasonable. We compare our mean M_* values to the sample investigated by Magdis et al. (2010) of LBGs at $z \sim 3$ with *Spitzer* data. Their mean stellar masses are $2.8 \times 10^{10} M_\odot$ and $4.2 \times 10^{10} M_\odot$, depending on which suite of models they use. Our mean values are $3.0 \times 10^{10} M_\odot$ for log-normal fitting and $6.7 \times 10^{10} M_\odot$ using our traditional SEDs. Their catalog also contains a few very bright, non-AGN sources that exceed $M_* \geq 5 \times 10^{11} M_\odot$, much like our own results (the hyperluminous sources). Although individual objects may suffer from systematic uncertainties in the M_* estimates, the CCPC as a whole is a reasonable match to other stellar mass studies of bright galaxies at high redshift.

5. SUMMARY

Although longitudinal data is required to perfectly map the evolution of galaxies (Abramson et al. 2016), astronomy must content itself with studies that contain as minimal inherent bias as possible. This manuscript details the *Spitzer* photometry of protocluster galaxies in the Candidate Cluster and Protocluster Catalog. The catalog probes galaxies between redshifts $2 < z < 6.6$

in dense environments. We built luminosity functions of the galaxies in various redshift bins at 3.6 and 4.5 μm wavelengths. These measure the rest-frame NIR emission of the galaxy populations to trace their stellar mass as a function of redshift.

The galaxies in both the field and CCPC samples contain extremely bright sources up to 5 magnitudes brighter than the characteristic magnitude m^* . These galaxies are divergent from the shape of the Schechter function, and exist at nearly all redshifts. Many of these are expected to be bright AGN and a few ($< 10\%$) low redshift interlopers. Semi-analytic models do not predict that these types of galaxies should exist (Guo et al. 2011), although they have been observed previously at similar redshifts (Pérez-González et al. 2008; Marchesini et al. 2009). Their nature is not yet established.

Field samples of galaxies are also photometrically measured, and remarkably the luminosity functions of the overdense regions are not statistically distinct from their field counterparts. In our current understanding of galaxy formation, the expectation is that the most massive galaxies at any epoch will be found in the densest environments. In Section 4 we analyzed a number of possibilities that might explain this phenomenon, but cannot find a satisfactory conclusion. We believe this to be the most fundamental result of this work.

We model the fitted LF parameter m^* as a function of redshift in the context of various stellar population models. By including the measurements at lower redshifts from Mancone et al. (2010) and Wylezalek et al. (2014), we find that a passively evolving stellar population formed in a single burst at high redshift ($z_f = 7-10$) is consistent with the data at all redshifts ($0.3 < z < 6.6$). An exponentially decaying star formation model with $\tau = 1$ Gyr is also in agreement with the data. Despite the fact that the majority of CCPC galaxies were spectroscopically selected based on their star forming properties (e.g. LBGs and line emitters) a constant star forming model is a poor fit to the observed $m^*(z)$.

A SED fitting technique has provided stellar mass estimates and some general information about the properties of the CCPC galaxies. We use supplemental *Hubble Space Telescope* data to probe the rest-frame optical emission to measure stellar colors for additional model constraints. However, we are careful to note that even with greater wavelength coverage than that which is presented here, SED fitting can be fraught with degeneracies (dust, age, metallicity) and inter-model uncertainties. Overall, the CCPC appears to be composed of $M \gtrsim 10^{10} M_\odot$ galaxies with mean formation redshifts $z_f > 7$. Apart from these broad statements, we cannot provide reliable dust content, metallicity information, or unique model fits to individual CCPC sources.

We thank the anonymous referee for helpful comments that improved the quality of this work. This work is based [in part] on observations made with the *Spitzer Space Telescope*, which is operated by the Jet Propulsion Laboratory, California Institute of Technology under a contract with NASA. This work has made use of the Rainbow Cosmological Surveys Database, which is operated by the Universidad Complutense de Madrid (UCM), partnered with the University of California Observatories at Santa Cruz (UCO/Lick, UCSC). This research has made use of the NASA/IPAC Extragalactic Database

(NED) which is operated by the Jet Propulsion Laboratory, California Institute of Technology, under contract with the National Aeronautics and Space Administration. Based on observations made with the NASA/ESA Hubble Space Telescope, and obtained from the Hubble Legacy Archive, which is a collaboration between the Space Telescope Science Institute (STScI/NASA), the Space Telescope European Coordinating Facility (ST-ECF/ESA) and the Canadian Astronomy Data Centre (CADC/NRC/CSA). This work is based on observations taken by the CANDELS Multi-Cycle Treasury Program with the NASA/ESA HST, which is operated by the Association of Universities for Research in Astronomy, Inc., under NASA contract NAS5-26555.

REFERENCES

- Abraham, R. G., et al. 2004, *AJ*, 127, 2455
- Abramson, L. E., Gladders, M. D., Dressler, A., Oemler, A., Poggianti, B., & Vulcani, B. 2016, *ArXiv e-prints*
- Adams, J. J., et al. 2011, *ApJS*, 192, 5
- Akiyama, M. 2005, *ApJ*, 629, 72
- Anderson, S. F., & Margon, B. 1987, *ApJ*, 314, 111
- Anderson, S. F., et al. 2001, *AJ*, 122, 503
- Ando, M., Ohta, K., Iwata, I., Watanabe, C., Tamura, N., Akiyama, M., & Aoki, K. 2004, *ApJ*, 610, 635
- Balestra, I., et al. 2010, *A&A*, 512, A12
- Balogh, M., et al. 2004, *MNRAS*, 348, 1355
- Barger, A. J., Cowie, L. L., Bautz, M. W., Brandt, W. N., Garmire, G. P., Hornschemeier, A. E., Ivison, R. J., & Owen, F. N. 2001a, *AJ*, 122, 2177
- Barger, A. J., Cowie, L. L., Brandt, W. N., Capak, P., Garmire, G. P., Hornschemeier, A. E., Steffen, A. T., & Wehner, E. H. 2002, *AJ*, 124, 1839
- Barger, A. J., Cowie, L. L., Mushotzky, R. F., & Richards, E. A. 2001b, *AJ*, 121, 662
- Barger, A. J., Cowie, L. L., & Richards, E. A. 2000, *AJ*, 119, 2092
- Barger, A. J., Cowie, L. L., & Wang, W.-H. 2008, *ApJ*, 689, 687
- Barger, A. J., et al. 2003, *AJ*, 126, 632
- Bauer, F. E., et al. 2002, *AJ*, 123, 1163
- Bertinocourt, B., et al. 2009, *ApJ*, 705, 68
- Bielby, R., et al. 2013, *MNRAS*, 430, 425
- Bolzonella, M., Miralles, J.-M., & Pelló, R. 2000, *A&A*, 363, 476
- Bond, N. A., Feldmeier, J. J., Matković, A., Gronwall, C., Ciardullo, R., & Gawiser, E. 2010, *ApJ*, 716, L200
- Bond, N. A., Gawiser, E., Guaita, L., Padilla, N., Gronwall, C., Ciardullo, R., & Lai, K. 2012, *ApJ*, 753, 95
- Bond, N. A., Gawiser, E., & Koekemoer, A. M. 2011, *ApJ*, 729, 48
- Bond, N. A., et al. 2014, *ApJ*, 791, 18
- Bonzini, M., et al. 2012, *ApJS*, 203, 15
- Bothwell, M. S., et al. 2013, *MNRAS*, 429, 3047
- Boutsia, K., et al. 2011, *ApJ*, 736, 41
- Bowler, R. A. A., et al. 2014, *MNRAS*, 440, 2810
- Brammer, G. B., van Dokkum, P. G., Illingworth, G. D., Bouwens, R. J., Labbé, I., Franx, M., Momcheva, I., & Oesch, P. A. 2013, *ApJ*, 765, L2
- Brodwin, M., et al. 2013, *ApJ*, 779, 138
- Brusa, M., et al. 2009a, *A&A*, 507, 1277
- . 2009b, *ApJ*, 693, 8
- . 2010, *ApJ*, 716, 348
- Bruzual, G., & Charlot, S. 2003, *MNRAS*, 344, 1000
- Buchner, J., et al. 2014, *A&A*, 564, A125
- Bunker, A. J., Stanway, E. R., Ellis, R. S., & McMahon, R. G. 2004, *MNRAS*, 355, 374
- Butcher, H., & Oemler, Jr., A. 1984, *ApJ*, 285, 426
- Campos, A., Yahil, A., Windhorst, R. A., Richards, E. A., Pascarelle, S., Impey, C., & Petry, C. 1999, *ApJ*, 511, L1
- Cantalupo, S., Lilly, S. J., & Porciani, C. 2007, *ApJ*, 657, 135
- Carilli, C. L., Riechers, D., Walter, F., Maiolino, R., Wagg, J., Lentati, L., McMahon, R., & Wolfe, A. 2013, *ApJ*, 763, 120
- Casey, C. M., Chapman, S. C., Smail, I., Alaghband-Zadeh, S., Bothwell, M. S., & Swinbank, A. M. 2011, *MNRAS*, 411, 2739
- Casey, C. M., et al. 2012, *ApJ*, 761, 139
- . 2015, *ApJ*, 808, L33
- Castro-Rodríguez, N., & López-Corredoira, M. 2012, *A&A*, 537, A31
- Chabrier, G. 2003, *PASP*, 115, 763
- Chapman, S. C., Scott, D., Windhorst, R. A., Frayer, D. T., Borys, C., Lewis, G. F., & Ivison, R. J. 2004a, *ApJ*, 606, 85
- Chapman, S. C., Smail, I., Blain, A. W., & Ivison, R. J. 2004b, *ApJ*, 614, 671
- Chapman, S. C., Smail, I., Windhorst, R., Muxlow, T., & Ivison, R. J. 2004c, *ApJ*, 611, 732
- Charlot, S., & Fall, S. M. 2000, *ApJ*, 539, 718
- Chiang, Y.-K., Overzier, R., & Gebhardt, K. 2013, *ApJ*, 779, 127
- Ciardullo, R., et al. 2012, *ApJ*, 744, 110
- Civano, F., et al. 2011, *ApJ*, 741, 91
- Colbert, J. W., Malkan, M. A., & Rich, R. M. 2006, *ApJ*, 648, 250
- Conselice, C. J., Bershad, M. A., Dickinson, M., & Papovich, C. 2003, *AJ*, 126, 1183
- Conselice, C. J., et al. 2011, *MNRAS*, 413, 80
- Contini, E., De Lucia, G., Hatch, N., Borgani, S., & Kang, X. 2015, *ArXiv e-prints*
- Cooke, E. A., Hatch, N. A., Muldrew, S. I., Rigby, E. E., & Kurk, J. D. 2014, *MNRAS*, 440, 3262
- Cooke, E. A., et al. 2015, *MNRAS*, 452, 2318
- Coppin, K. E. K., et al. 2008, *MNRAS*, 389, 45
- . 2010, *MNRAS*, 407, L103
- Cowie, L. L., Barger, A. J., Hu, E. M., Capak, P., & Songaila, A. 2004, *AJ*, 127, 3137
- Cowie, L. L., Songaila, A., Hu, E. M., & Cohen, J. G. 1996, *AJ*, 112, 839
- Cowie, L. L., Songaila, A., Kim, T.-S., & Hu, E. M. 1995, *AJ*, 109, 1522
- Cristiani, S., & D'Odorico, V. 2000, *AJ*, 120, 1648
- Cristiani, S., et al. 2000, *A&A*, 359, 489
- Croft, S., Kurk, J., van Breugel, W., Stanford, S. A., de Vries, W., Pentericci, L., & Röttgering, H. 2005, *AJ*, 130, 867
- Curtis-Lake, E., et al. 2012, *MNRAS*, 422, 1425
- Daddi, E., Dannerbauer, H., Krips, M., Walter, F., Dickinson, M., Elbaz, D., & Morrison, G. E. 2009, *ApJ*, 695, L176
- Daddi, E., et al. 2005, *ApJ*, 626, 680
- Dannerbauer, H., Lehnert, M. D., Lutz, D., Tacconi, L., Bertoldi, F., Carilli, C., Genzel, R., & Menten, K. M. 2004, *ApJ*, 606, 664
- Dannerbauer, H., et al. 2006, *ApJ*, 637, L5
- Davies, L. J. M., Bremer, M. N., Stanway, E. R., Birkinshaw, M., & Lehnert, M. D. 2010, *MNRAS*, 408, L31
- Dawson, S., Rhoads, J. E., Malhotra, S., Stern, D., Wang, J., Dey, A., Spinrad, H., & Jannuzi, B. T. 2007, *ApJ*, 671, 1227
- Dawson, S., Spinrad, H., Stern, D., Dey, A., van Breugel, W., de Vries, W., & Reuland, M. 2002, *ApJ*, 570, 92
- Dawson, S., Stern, D., Bunker, A. J., Spinrad, H., & Dey, A. 2001, *AJ*, 122, 598
- Dawson, S., et al. 2004, *ApJ*, 617, 707
- De Breuck, C., et al. 2004, *A&A*, 424, 1
- de Bruyn, A. G., O'Dea, C. P., & Baum, S. A. 1996, *A&A*, 305, 450
- Dey, A., Lee, K.-S., Reddy, N., Cooper, M., Inami, H., Hong, S., Gonzalez, A. H., & Jannuzi, B. T. 2016, *ApJ*, 823, 11
- Diener, C., et al. 2013, *ApJ*, 765, 109
- . 2015, *ApJ*, 802, 31
- Digby-North, J. A., et al. 2010, *MNRAS*, 407, 846
- Dijkstra, M., & Westra, E. 2010, *MNRAS*, 401, 2343
- Djorgovski, S. G., Stern, D., Mahabal, A. A., & Brunner, R. 2003, *ApJ*, 596, 67
- Dobrzycki, A., & Bechtold, J. 1996, *ApJ*, 457, 102
- Doherty, M., et al. 2010, *A&A*, 509, A83
- Donley, J. L., Rieke, G. H., Alexander, D. M., Egami, E., & Pérez-González, P. G. 2010, *ApJ*, 719, 1393
- Donley, J. L., Rieke, G. H., Pérez-González, P. G., Rigby, J. R., & Alonso-Herrero, A. 2007, *ApJ*, 660, 167
- Dow-Hygelund, C. C., et al. 2007, *ApJ*, 660, 47
- Dressler, A. 1980, *ApJ*, 236, 351
- Eales, S., Bertoldi, F., Ivison, R., Carilli, C., Dunne, L., & Owen, F. 2003, *MNRAS*, 344, 169
- Eisenhardt, P. R. M., et al. 2008, *ApJ*, 684, 905
- Ellison, S. L., Pettini, M., Steidel, C. C., & Shapley, A. E. 2001, *ApJ*, 549, 770
- Elmegreen, B. G., & Elmegreen, D. M. 2010, *ApJ*, 722, 1895
- Elston, R., Bechtold, J., Hill, G. J., & Ge, J. 1996, *ApJ*, 456, L13

- Erb, D. K., Bogosavljević, M., & Steidel, C. C. 2011, *ApJ*, 740, L31
- Erb, D. K., Shapley, A. E., Steidel, C. C., Pettini, M., Adelberger, K. L., Hunt, M. P., Moorwood, A. F. M., & Cuby, J.-G. 2003, *ApJ*, 591, 101
- Erb, D. K., Steidel, C. C., Shapley, A. E., Pettini, M., & Adelberger, K. L. 2004, *ApJ*, 612, 122
- Erb, D. K., Steidel, C. C., Shapley, A. E., Pettini, M., Reddy, N. A., & Adelberger, K. L. 2006, *ApJ*, 646, 107
- Faber, S. M., et al. 2007, *ApJ*, 665, 265
- Fasano, G., Cristiani, S., Arnouts, S., & Filippi, M. 1998, *AJ*, 115, 1400
- Fassbender, R., et al. 2014, *A&A*, 568, A5
- Fernández-Soto, A., Lanzetta, K. M., Chen, H.-W., Pascarelle, S. M., & Yahata, N. 2001, *ApJS*, 135, 41
- Fernández-Soto, A., Lanzetta, K. M., & Yahil, A. 1999, *ApJ*, 513, 34
- Feruglio, C., Daddi, E., Fiore, F., Alexander, D. M., Piconcelli, E., & Malacaria, C. 2011, *ApJ*, 729, L4
- Finkelstein, S. L., Malhotra, S., Rhoads, J. E., Hathi, N. P., & Pirzkal, N. 2009a, *MNRAS*, 393, 1174
- Finkelstein, S. L., Rhoads, J. E., Malhotra, S., & Grogan, N. 2009b, *ApJ*, 691, 465
- Finkelstein, S. L., et al. 2011, *ApJ*, 735, 5
- Finlator, K., Davé, R., & Oppenheimer, B. D. 2007, *MNRAS*, 376, 1861
- Fiore, F., et al. 2012, *A&A*, 537, A16
- Fontanot, F., Cristiani, S., Monaco, P., Nonino, M., Vanzella, E., Brandt, W. N., Grazian, A., & Mao, J. 2007, *A&A*, 461, 39
- Franck, J. R., & McGaugh, S. S. 2016a, *ArXiv e-prints*
- . 2016b, *ApJ*, 817, 158
- Fritz, A., et al. 2014, *A&A*, 563, A92
- Fynbo, J. P. U., Ledoux, C., Möller, P., Thomsen, B., & Burud, I. 2003a, *A&A*, 407, 147
- Fynbo, J. P. U., Ledoux, C., Möller, P., Thomsen, B., & Burud, I. 2003b, *A&A*, 407, 147
- Fynbo, J. U., Möller, P., & Thomsen, B. 2001, *A&A*, 374, 443
- Galametz, A., et al. 2013, *A&A*, 559, A2
- Gavignaud, I., et al. 2006, *A&A*, 457, 79
- . 2008, *A&A*, 492, 637
- Georgakakis, A., et al. 2006, *MNRAS*, 371, 221
- Georgantopoulos, I., Rovilos, E., Xilouris, E. M., Comastri, A., & Akylas, A. 2011, *A&A*, 526, A86
- Gladders, M. D., Oemler, A., Dressler, A., Poggianti, B., Vulcani, B., & Abramson, L. 2013, *ApJ*, 770, 64
- Gnerucci, A., et al. 2011, *A&A*, 528, A88
- Gobat, R., et al. 2011, *A&A*, 526, A133
- . 2012, *ApJ*, 759, L44
- . 2013, *ApJ*, 776, 9
- Grazian, A., et al. 2006, *A&A*, 449, 951
- . 2012, *A&A*, 547, A51
- Grogan, N. A., et al. 2011, *ApJS*, 197, 35
- Grove, L. F., Fynbo, J. P. U., Ledoux, C., Limousin, M., Möller, P., Nilsson, K. K., & Thomsen, B. 2009, *A&A*, 497, 689
- Gunn, J. E., & Gott, III, J. R. 1972, *ApJ*, 176, 1
- Guo, Q., et al. 2011, *MNRAS*, 413, 101
- Hainline, K. N., Shapley, A. E., Greene, J. E., & Steidel, C. C. 2011, *ApJ*, 733, 31
- Hainline, L. J., Blain, A. W., Greve, T. R., Chapman, S. C., Smail, I., & Ivison, R. J. 2006, *ApJ*, 650, 614
- Hamann, F., Barlow, T. A., & Junkkarinen, V. 1997, *ApJ*, 478, 87
- Harrison, C. M., et al. 2012, *MNRAS*, 426, 1073
- Hatch, N. A., Cooke, E. A., Muldrew, S. I., Hartley, W. G., Almaini, O., Conselice, C. J., & Simpson, C. J. 2016, *MNRAS*
- Hatch, N. A., Kurk, J. D., Pentericci, L., Venemans, B. P., Kuiper, E., Miley, G. K., & Röttgering, H. J. A. 2011, *MNRAS*, 415, 2993
- Hathi, N. P., Malhotra, S., & Rhoads, J. E. 2008, *ApJ*, 673, 686
- Hawkins, M. R. S., & Veron, P. 1993, *MNRAS*, 260, 202
- Hayashi, M., Kodama, T., Koyama, Y., Tadaki, K.-I., & Tanaka, I. 2011, *MNRAS*, 415, 2670
- Hayashi, M., Kodama, T., Tadaki, K.-i., Koyama, Y., & Tanaka, I. 2012, *ApJ*, 757, 15
- Hayashi, M., et al. 2009, *ApJ*, 691, 140
- Hayashino, T., et al. 2004, *AJ*, 128, 2073
- Henry, A. L., Martin, C. L., Dressler, A., Sawicki, M., & McCarthy, P. 2012, *ApJ*, 744, 149
- Hewett, P. C., & Wild, V. 2010, *MNRAS*, 405, 2302
- Hornschemeier, A. E., et al. 2001, *ApJ*, 554, 742
- Hu, E. M., Cowie, L. L., Barger, A. J., Capak, P., Kakazu, Y., & Trouille, L. 2010, *ApJ*, 725, 394
- Hu, E. M., Cowie, L. L., Capak, P., McMahon, R. G., Hayashino, T., & Komiyama, Y. 2004, *AJ*, 127, 563
- Hu, E. M., McMahon, R. G., & Cowie, L. L. 1999, *ApJ*, 522, L9
- Hu, E. M., McMahon, R. G., & Egami, E. 1996, *ApJ*, 459, L53
- Husband, K., Bremer, M. N., Stanway, E. R., Davies, L. J. M., Lehnert, M. D., & Douglas, L. S. 2013, *MNRAS*, 432, 2869
- Inoue, A. K., et al. 2011, *MNRAS*, 411, 2336
- Ivison, R. J., Papadopoulos, P. P., Smail, I., Greve, T. R., Thomson, A. P., Xilouris, E. M., & Chapman, S. C. 2011, *MNRAS*, 412, 1913
- Iwata, I., Inoue, A. K., & Burgarella, D. 2005, *A&A*, 440, 881
- Iwata, I., Ohta, K., Tamura, N., Akiyama, M., Aoki, K., Ando, M., Kiuchi, G., & Sawicki, M. 2007, *MNRAS*, 376, 1557
- Iye, M., et al. 2006, *Nature*, 443, 186
- Jangren, A., Wegner, G., Salzer, J. J., Werk, J. K., & Gronwall, C. 2005, *AJ*, 130, 496
- Jiang, L., et al. 2011, *ApJ*, 743, 65
- . 2013, *ApJ*, 772, 99
- Kajino, H., et al. 2009, *ApJ*, 704, 117
- Kakazu, Y., Cowie, L. L., & Hu, E. M. 2007, *ApJ*, 668, 853
- Kashikawa, N., et al. 2006, *ApJ*, 648, 7
- . 2011, *ApJ*, 734, 119
- Keel, W. C., Wu, W., Waddington, I., Windhorst, R. A., & Pascarelle, S. M. 2002, *AJ*, 123, 3041
- Kilic, M., Mendez, R. A., von Hippel, T., & Winget, D. E. 2005, *ApJ*, 633, 1126
- Kirkpatrick, A., et al. 2012, *ApJ*, 759, 139
- Knudsen, K. K., van der Werf, P. P., & Kneib, J.-P. 2008, *MNRAS*, 384, 1611
- Kocevski, D. D., Lubin, L. M., Gal, R., Lemaux, B. C., Fassnacht, C. D., & Squires, G. K. 2009, *ApJ*, 690, 295
- Kriek, M., et al. 2008, *ApJ*, 677, 219
- Kroupa, P. 2002, *Science*, 295, 82
- Krumpe, M., et al. 2008, *A&A*, 483, 415
- Kulas, K. R., Shapley, A. E., Kollmeier, J. A., Zheng, Z., Steidel, C. C., & Hainline, K. N. 2012, *ApJ*, 745, 33
- Kurk, J. D., Pentericci, L., Overzier, R. A., Röttgering, H. J. A., & Miley, G. K. 2004a, *A&A*, 428, 817
- Kurk, J. D., Pentericci, L., Röttgering, H. J. A., & Miley, G. K. 2004b, *A&A*, 428, 793
- Lanzetta, K. M., Yahil, A., & Fernández-Soto, A. 1996, *Nature*, 381, 759
- Larson, R. B., Tinsley, B. M., & Caldwell, C. N. 1980, *ApJ*, 237, 692
- Law, D. R., Steidel, C. C., Shapley, A. E., Nagy, S. R., Reddy, N. A., & Erb, D. K. 2012, *ApJ*, 745, 85
- Le Fevre, O., Deltorn, J. M., Crampton, D., & Dickinson, M. 1996, *ApJ*, 471, L11
- Le Fèvre, O., et al. 2004, *A&A*, 428, 1043
- . 2005, *A&A*, 439, 845
- Lehmer, B. D., et al. 2009a, *ApJ*, 691, 687
- . 2009b, *MNRAS*, 400, 299
- Lemaux, B. C., et al. 2009, *ApJ*, 700, 20
- Lemoine-Busserolle, M., Bunker, A., Lamareille, F., & Kissler-Patig, M. 2010, *MNRAS*, 401, 1657
- Lilly, S. J., et al. 2007, *ApJS*, 172, 70
- Lowenthal, J. D., Koo, D. C., Simard, L., & van Kampen, E. 2009, *ApJ*, 703, 198
- Lowenthal, J. D., et al. 1997, *ApJ*, 481, 673
- Lu, L., Sargent, W. L. W., & Barlow, T. A. 1998, *AJ*, 115, 55
- Luo, B., et al. 2008, *ApJS*, 179, 19
- Ly, C., et al. 2009, *ApJ*, 697, 1410
- Madau, P., & Dickinson, M. 2014, *ARA&A*, 52, 415
- Magdis, G. E., Rigopoulou, D., Huang, J.-S., & Fazio, G. G. 2010, *MNRAS*, 401, 1521
- Mainieri, V., et al. 2008, *ApJS*, 179, 95
- Maiolino, R., Caselli, P., Nagao, T., Walmsley, M., De Breuck, C., & Meneghetti, M. 2009, *A&A*, 500, L1
- Malhotra, S., et al. 2005, *ApJ*, 626, 666
- Mancone, C. L., & Gonzalez, A. H. 2012, *PASP*, 124, 606
- Mancone, C. L., Gonzalez, A. H., Brodwin, M., Stanford, S. A., Eisenhardt, P. R. M., Stern, D., & Jones, C. 2010, *ApJ*, 720, 284

- Marchesini, D., van Dokkum, P. G., Förster Schreiber, N. M., Franx, M., Labbé, I., & Wuyts, S. 2009, *ApJ*, 701, 1765
- Martin, C. L., Sawicki, M., Dressler, A., & McCarthy, P. 2008, *ApJ*, 679, 942
- Maschietto, F., et al. 2008, *MNRAS*, 389, 1223
- Matsuda, Y., et al. 2011, *MNRAS*, 416, 2041
- McCarthy, P. J., Kapahi, V. K., van Breugel, W., Persson, S. E., Athreya, R., & Subrahmanya, C. R. 1996, *ApJS*, 107, 19
- McGaugh, S. S. 1996, *MNRAS*, 280, 337
- McIntosh, D. H., Impey, C. D., & Petry, C. E. 2004, *AJ*, 128, 544
- McLure, R. J., et al. 2006, *MNRAS*, 372, 357
- Mehlert, D., et al. 2002, *A&A*, 393, 809
- Mei, S., et al. 2009, *ApJ*, 690, 42
- Melnyk, O., et al. 2013, *A&A*, 557, A81
- Menéndez-Delmestre, K., et al. 2009, *ApJ*, 699, 667
- Mignoli, M., et al. 2005, *A&A*, 437, 883
- Mihos, J. C., & Hernquist, L. 1996, *ApJ*, 464, 641
- Møller, P., & Fynbo, J. U. 2001, *A&A*, 372, L57
- Moore, B., Katz, N., Lake, G., Dressler, A., & Oemler, A. 1996, *Nature*, 379, 613
- Moorwood, A. F. M., van der Werf, P. P., Cuby, J. G., & Oliva, E. 2000, *A&A*, 362, 9
- Moth, P., & Elston, R. J. 2002, *AJ*, 124, 1886
- Muldrew, S. I., Hatch, N. A., & Cooke, E. A. 2015, *MNRAS*, 452, 2528
- Murayama, T., et al. 2007, *ApJS*, 172, 523
- Nagao, T., et al. 2004, *ApJ*, 613, L9
- . 2005, *ApJ*, 634, 142
- . 2007, *A&A*, 468, 877
- Neri, R., Downes, D., Cox, P., & Walter, F. 2014, *A&A*, 562, A35
- Nestor, D. B., Shapley, A. E., Steidel, C. C., & Siana, B. 2011, *ApJ*, 736, 18
- Noiro, G., et al. 2016, *ArXiv e-prints*
- Noll, S., et al. 2004, *A&A*, 418, 885
- Oemler, Jr., A., Dressler, A., Gladders, M. G., Fritz, J., Poggianti, B. M., Vulcani, B., & Abramson, L. 2013, *ApJ*, 770, 63
- Ono, Y., et al. 2012, *ApJ*, 744, 83
- Onodera, M., Arimoto, N., Daddi, E., Renzini, A., Kong, X., Cimatti, A., Broadhurst, T., & Alexander, D. M. 2010, *ApJ*, 715, 385
- Osmer, P. S., Porter, A. C., & Green, R. F. 1994, *ApJ*, 436, 678
- Ouchi, M., et al. 2004a, *ApJ*, 611, 660
- . 2004b, *ApJ*, 611, 685
- . 2005, *ApJ*, 620, L1
- . 2008, *ApJS*, 176, 301
- . 2009, *ApJ*, 696, 1164
- . 2010, *ApJ*, 723, 869
- Owensworth, J. R., Conselice, C. J., Mundy, C. J., Mortlock, A., Hartley, W. G., Duncan, K., & Almaini, O. 2016, *ArXiv e-prints*
- Papovich, C., Dickinson, M., & Ferguson, H. C. 2001a, *ApJ*, 559, 620
- . 2001b, *ApJ*, 559, 620
- Papovich, C., Dickinson, M., Giavalisco, M., Conselice, C. J., & Ferguson, H. C. 2005, *ApJ*, 631, 101
- Papovich, C., et al. 2010, *ApJ*, 716, 1503
- . 2012, *ApJ*, 750, 93
- Park, S. Q., et al. 2010, *ApJ*, 717, 1181
- Patnaik, A. R., Browne, I. W. A., Walsh, D., Chaffee, F. H., & Foltz, C. B. 1992, *MNRAS*, 259, 1P
- Peng, Y.-j., et al. 2010, *ApJ*, 721, 193
- Pentericci, L., Kurk, J. D., Carilli, C. L., Harris, D. E., Miley, G. K., & Röttgering, H. J. A. 2002, *A&A*, 396, 109
- Pentericci, L., et al. 2000, *A&A*, 361, L25
- . 2011, *ApJ*, 743, 132
- Percival, S. M., Salaris, M., Cassisi, S., & Pietrinferni, A. 2009, *ApJ*, 690, 427
- Pérez-González, P. G., et al. 2008, *ApJ*, 675, 234
- Péroux, C., Storrie-Lombardi, L. J., McMahon, R. G., Irwin, M., & Hook, I. M. 2001, *AJ*, 121, 1799
- Peter, A. H. G., Shapley, A. E., Law, D. R., Steidel, C. C., Erb, D. K., Reddy, N. A., & Pettini, M. 2007, *ApJ*, 668, 23
- Petitjean, P., & Srianand, R. 1999, *A&A*, 345, 73
- Petry, C. E., Impey, C. D., & Foltz, C. B. 1998, *ApJ*, 494, 60
- Phillips, A. C., Guzmán, R., Gallego, J., Koo, D. C., Lowenthal, J. D., Vogt, N. P., Faber, S. M., & Illingworth, G. D. 1997, *ApJ*, 489, 543
- Pirzkal, N., et al. 2013, *ApJ*, 772, 48
- Polletta, M., et al. 2008, *A&A*, 492, 81
- Pope, A., et al. 2006, *MNRAS*, 370, 1185
- Postman, M., Lubin, L. M., & Oke, J. B. 2001, *AJ*, 122, 1125
- Rafelski, M., Wolfe, A. M., & Chen, H.-W. 2011, *ApJ*, 736, 48
- Rafelski, M., Wolfe, A. M., Cooke, J., Chen, H.-W., Armandroff, T. E., & Wirth, G. D. 2009, *ApJ*, 703, 2033
- Raiter, A., Fosbury, R. A. E., & Teimoorinia, H. 2010, *A&A*, 510, A109
- Rakos, K. D., & Schombert, J. M. 1995, *ApJ*, 439, 47
- Ramos Almeida, C., Rodríguez Espinosa, J. M., Barro, G., Gallego, J., & Pérez-González, P. G. 2009, *AJ*, 137, 179
- Ranalli, P., et al. 2013, *A&A*, 555, A42
- Rangel, C., et al. 2014, *MNRAS*, 440, 3630
- Reddy, N. A., Steidel, C. C., Erb, D. K., Shapley, A. E., & Pettini, M. 2006, *ApJ*, 653, 1004
- Reimers, D., Clavel, J., Groote, D., Engels, D., Hagen, H. J., Naylor, T., Wamsteker, W., & Hopp, U. 1989, *A&A*, 218, 71
- Reshetnikov, V. P., & Vasil'Ev, A. A. 2002, *Astronomy Letters*, 28, 1
- Rhoads, J. E., et al. 2004, *ApJ*, 611, 59
- . 2005, *ApJ*, 621, 582
- . 2009, *ApJ*, 697, 942
- Riechers, D. A., et al. 2006, *ApJ*, 650, 604
- . 2011, *ApJ*, 733, L11
- Rigby, J. R., et al. 2008, *ApJ*, 675, 262
- Rodney, S. A., et al. 2014, *AJ*, 148, 13
- Rodríguez-Pascual, P. M., de La Fuente, A., Sanz, J. L., Recondo, M. C., Clavel, J., Santos-Lleo, M., & Wamsteker, W. 1995, *ApJ*, 448, 575
- Roettgering, H. J. A., van Ojik, R., Miley, G. K., Chambers, K. C., van Breugel, W. J. M., & de Koff, S. 1997, *A&A*, 326, 505
- Ross, N. P., et al. 2012, *ApJS*, 199, 3
- Röttgering, H. J. A., Hunstead, R. W., Miley, G. K., van Ojik, R., & Wieringa, M. H. 1995, *MNRAS*, 277, 389
- Saito, T., Shimasaku, K., Okamura, S., Ouchi, M., Akiyama, M., & Yoshida, M. 2006, *ApJ*, 648, 54
- Saito, T., Shimasaku, K., Okamura, S., Ouchi, M., Akiyama, M., Yoshida, M., & Ueda, Y. 2008, *ApJ*, 675, 1076
- Salimbeni, S., et al. 2009, *A&A*, 501, 865
- Sand, D. J., Treu, T., Ellis, R. S., & Smith, G. P. 2005, *ApJ*, 627, 32
- Santini, P., et al. 2009, *A&A*, 504, 751
- Santos, M. R., Ellis, R. S., Kneib, J.-P., Richard, J., & Kuijken, K. 2004, *ApJ*, 606, 683
- Sarajedini, V. L., Koo, D. C., Klesman, A. J., Laird, E. S., Perez Gonzalez, P. G., & Mozena, M. 2011, *ApJ*, 731, 97
- Savaglio, S., Cristiani, S., D'Odorico, S., Fontana, A., Giallongo, E., & Molaro, P. 1997, *A&A*, 318, 347
- Savaglio, S., D'Odorico, S., & Moller, P. 1994, *A&A*, 281, 331
- Schaye, J., Theuns, T., Rauch, M., Efstathiou, G., & Sargent, W. L. W. 2000, *MNRAS*, 318, 817
- Schechter, P. 1976, *ApJ*, 203, 297
- Schenker, M. A., Stark, D. P., Ellis, R. S., Robertson, B. E., Dunlop, J. S., McLure, R. J., Kneib, J.-P., & Richard, J. 2012, *ApJ*, 744, 179
- Schneider, D. P., Schmidt, M., & Gunn, J. E. 1991, *AJ*, 101, 2004
- Schombert, J., & Rakos, K. 2009, *ApJ*, 699, 1530
- Schreier, E. J., et al. 2001, *ApJ*, 560, 127
- Scott, J., Bechtold, J., & Dobrzycki, A. 2000, *ApJS*, 130, 37
- Sealey, K. M., Drinkwater, M. J., & Webb, J. K. 1998, *ApJ*, 499, L135
- Shapley, A. E., Erb, D. K., Pettini, M., Steidel, C. C., & Adelberger, K. L. 2004, *ApJ*, 612, 108
- Shapley, A. E., Steidel, C. C., Adelberger, K. L., Dickinson, M., Giavalisco, M., & Pettini, M. 2001, *ApJ*, 562, 95
- Shapley, A. E., Steidel, C. C., Erb, D. K., Reddy, N. A., Adelberger, K. L., Pettini, M., Barmby, P., & Huang, J. 2005, *ApJ*, 626, 698
- Shapley, A. E., Steidel, C. C., Pettini, M., Adelberger, K. L., & Erb, D. K. 2006, *ApJ*, 651, 688
- Sharp, R. G., Sabbage, C. N., Vivas, A. K., Oemler, A., McMahon, R. G., Hodgkin, S. T., & Coppi, P. S. 2002, *MNRAS*, 337, 1153
- Shim, H., Chary, R.-R., Dickinson, M., Lin, L., Spinrad, H., Stern, D., & Yan, C.-H. 2011, *ApJ*, 738, 69
- Shimasaku, K., et al. 2006, *PASJ*, 58, 313

- Silverman, J. D., et al. 2005, *ApJ*, 618, 123
- . 2010, *ApJS*, 191, 124
- Simcoe, R. A., Sargent, W. L. W., Rauch, M., & Becker, G. 2006, *ApJ*, 637, 648
- Simpson, J. M., et al. 2014, *ApJ*, 788, 125
- Skelton, R. E., et al. 2014, *ApJS*, 214, 24
- Smail, I., Chapman, S. C., Blain, A. W., & Ivison, R. J. 2004, *ApJ*, 616, 71
- Söchting, I. K., Coldwell, G. V., Clowes, R. G., Campusano, L. E., & Graham, M. J. 2012, *MNRAS*, 423, 2436
- Song, M., et al. 2014, *ApJ*, 791, 3
- Songaila, A. 1998, *AJ*, 115, 2184
- Spinrad, H., Stern, D., Bunker, A., Dey, A., Lanzetta, K., Yahil, A., Pascarelle, S., & Fernández-Soto, A. 1998, *AJ*, 116, 2617
- Spitler, L. R., et al. 2014, *ApJ*, 787, L36
- Srianand, R. 1996, *ApJ*, 462, 68
- Stalin, C. S., Petitjean, P., Srianand, R., Fox, A. J., Coppolani, F., & Schwobe, A. 2010, *MNRAS*, 401, 294
- Stanford, S. A., Dickinson, M., Postman, M., Ferguson, H. C., Lucas, R. A., Conselice, C. J., Budavári, T., & Somerville, R. 2004, *AJ*, 127, 131
- Stanford, S. A., Eisenhardt, P. R., & Dickinson, M. 1998, *ApJ*, 492, 461
- Stanford, S. A., Eisenhardt, P. R. M., & Dickinson, M. 1995, *ApJ*, 450, 512
- Stanway, E. R., Bunker, A. J., McMahon, R. G., Ellis, R. S., Treu, T., & McCarthy, P. J. 2004a, *ApJ*, 607, 704
- Stanway, E. R., et al. 2004b, *ApJ*, 604, L13
- . 2007, *MNRAS*, 376, 727
- Stark, D. P., Ellis, R. S., & Ouchi, M. 2011, *ApJ*, 728, L2
- Stark, D. P., Schenker, M. A., Ellis, R., Robertson, B., McLure, R., & Dunlop, J. 2013, *ApJ*, 763, 129
- Steidel, C. C., Adelberger, K. L., Dickinson, M., Giavalisco, M., Pettini, M., & Kellogg, M. 1998, *ApJ*, 492, 428
- Steidel, C. C., Adelberger, K. L., Giavalisco, M., Dickinson, M., & Pettini, M. 1999, *ApJ*, 519, 1
- Steidel, C. C., Adelberger, K. L., Shapley, A. E., Pettini, M., Dickinson, M., & Giavalisco, M. 2000, *ApJ*, 532, 170
- . 2003, *ApJ*, 592, 728
- Steidel, C. C., Shapley, A. E., Pettini, M., Adelberger, K. L., Erb, D. K., Reddy, N. A., & Hunt, M. P. 2004, *ApJ*, 604, 534
- Steinhardt, C. L., Capak, P., Masters, D., & Speagle, J. S. 2016, *ApJ*, 824, 21
- Stern, D., & Spinrad, H. 1999, *PASP*, 111, 1475
- Storrie-Lombardi, L. J., McMahon, R. G., Irwin, M. J., & Hazard, C. 1996, *ApJ*, 468, 121
- Storrie-Lombardi, L. J., & Wolfe, A. M. 2000, *ApJ*, 543, 552
- Straughn, A. N., et al. 2008, *AJ*, 135, 1624
- . 2011, *AJ*, 141, 14
- Swinbank, A. M., Smail, I., Chapman, S. C., Blain, A. W., Ivison, R. J., & Keel, W. C. 2004, *ApJ*, 617, 64
- Szokoly, G. P., et al. 2004, *ApJS*, 155, 271
- Tadaki, K.-I., Kodama, T., Koyama, Y., Hayashi, M., Tanaka, I., & Tokoku, C. 2011, *PASJ*, 63, 437
- Tan, Q., et al. 2014, *A&A*, 569, A98
- Tanaka, M., et al. 2013, *ApJ*, 772, 113
- Tang, Y., Giavalisco, M., Guo, Y., & Kurk, J. 2014, *ApJ*, 793, 92
- Taniguchi, Y., et al. 2005, *PASJ*, 57, 165
- . 2009, *ApJ*, 701, 915
- Tanner, A. M., Bechtold, J., Walker, C. E., Black, J. H., & Cutri, R. M. 1996, *AJ*, 112, 62
- Tapken, C., Appenzeller, I., Noll, S., Richling, S., Heidt, J., Meinköhn, E., & Mehlert, D. 2007, *A&A*, 467, 63
- Tapken, C., et al. 2006, *A&A*, 455, 145
- Teplitz, H. I., et al. 2007, *ApJ*, 659, 941
- Tinsley, B. M. 1972, *A&A*, 20, 383
- Tody, D. 1986, in *Society of Photo-Optical Instrumentation Engineers (SPIE) Conference Series*, Vol. 627, *Instrumentation in astronomy VI*, ed. D. L. Crawford, 733
- Tody, D. 1993, in *Astronomical Society of the Pacific Conference Series*, Vol. 52, *Astronomical Data Analysis Software and Systems II*, ed. R. J. Hanisch, R. J. V. Brissenden, & J. Barnes, 173
- Toshikawa, J., et al. 2014, *ApJ*, 792, 15
- . 2016, *ApJ*, 826, 114
- Tozzi, P., et al. 2009, *ApJ*, 698, 740
- Tran, K.-V. H., van Dokkum, P., Illingworth, G. D., Kelson, D., Gonzalez, A., & Franx, M. 2005, *ApJ*, 619, 134
- Treister, E., et al. 2009, *ApJ*, 693, 1713
- Tripp, T. M., Lu, L., & Savage, B. D. 1997, *ApJS*, 112, 1
- Trouille, L., Barger, A. J., Cowie, L. L., Yang, Y., & Mushotzky, R. F. 2008, *ApJS*, 179, 1
- Trump, J. R., et al. 2009, *ApJ*, 696, 1195
- . 2011, *ApJ*, 743, 144
- . 2014, *ApJ*, 793, 101
- van Breukelen, C., Jarvis, M. J., & Venemans, B. P. 2005, *MNRAS*, 359, 895
- van Dokkum, P. G. 2005, *AJ*, 130, 2647
- van Dokkum, P. G., & Franx, M. 2001, *ApJ*, 553, 90
- van Dokkum, P. G., et al. 2006, *ApJ*, 638, L59
- Vanzella, E., et al. 2002, *A&A*, 396, 847
- . 2004, *A&A*, 423, 761
- . 2005, *A&A*, 434, 53
- . 2006, *A&A*, 454, 423
- . 2008, *A&A*, 478, 83
- . 2010, *ApJ*, 725, 1011
- Venemans, B. P., et al. 2002, *ApJ*, 569, L11
- . 2005, *A&A*, 431, 793
- . 2007, *A&A*, 461, 823
- Vernet, J., & Cimatti, A. 2001, *A&A*, 380, 409
- Veron, P., & Hawkins, M. R. S. 1995, *A&A*, 296, 665
- Vogel, S., & Reimers, D. 1995, *A&A*, 294, 377
- Wampler, E. J., Williger, G. M., Baldwin, J. A., Carswell, R. F., Hazard, C., & McMahon, R. G. 1996, *A&A*, 316, 33
- Wang, J.-X., Malhotra, S., Rhoads, J. E., Zhang, H.-T., & Finkelstein, S. L. 2009, *ApJ*, 706, 762
- Wang, T., et al. 2016, *ArXiv e-prints*
- Wang, W.-H., Cowie, L. L., & Barger, A. J. 2004, *ApJ*, 613, 655
- . 2006, *ApJ*, 647, 74
- Watabe, Y., Risaliti, G., Salvati, M., Nardini, E., Sani, E., & Marconi, A. 2009, *MNRAS*, 396, L1
- Webb, T. M. A., Lilly, S. J., Clements, D. L., Eales, S., Yun, M., Brodwin, M., Dunne, L., & Gear, W. K. 2003, *ApJ*, 597, 680
- Webb, T. M. A., et al. 2006, *ApJ*, 636, L17
- Weiner, B. J., et al. 2005, *ApJ*, 620, 595
- Weymann, R. J., Stern, D., Bunker, A., Spinrad, H., Chaffee, F. H., Thompson, R. I., & Storrie-Lombardi, L. J. 1998, *ApJ*, 505, L95
- Whitaker, K. E., et al. 2011, *ApJ*, 735, 86
- Wirth, G. D., et al. 2004, *AJ*, 127, 3121
- Wolf, C., et al. 1999, *A&A*, 343, 399
- Wolfe, A. M., & Prochaska, J. X. 2000, *ApJ*, 545, 591
- Worseck, G., & Wisotzki, L. 2006, *A&A*, 450, 495
- Worseck, G., Wisotzki, L., & Selman, F. 2008, *A&A*, 487, 539
- Wuyts, S., Labbé, I., Förster Schreiber, N. M., Franx, M., Rudnick, G., Brammer, G. B., & van Dokkum, P. G. 2008, *ApJ*, 682, 985
- Wuyts, S., van Dokkum, P. G., Franx, M., Förster Schreiber, N. M., Illingworth, G. D., Labbé, I., & Rudnick, G. 2009, *ApJ*, 706, 885
- Wuyts, S., et al. 2007, *ApJ*, 655, 51
- Wylezalek, D., et al. 2013, *ApJ*, 769, 79
- . 2014, *ApJ*, 786, 17
- Xu, C., et al. 2007, *AJ*, 134, 169
- Xue, Y. Q., et al. 2010, *ApJ*, 720, 368
- Yang, Y., Zabludoff, A., Jahnke, K., Eisenstein, D., Davé, R., Shectman, S. A., & Kelson, D. D. 2011, *ApJ*, 735, 87
- York, D. G., Yanny, B., Crotts, A., Carilli, C., Garrison, E., & Matheson, L. 1991, *MNRAS*, 250, 24
- Yoshida, M., et al. 2006, *ApJ*, 653, 988
- Yoshikawa, T., et al. 2010, *ApJ*, 718, 112
- Zhao, D., Conselice, C. J., Aragón-Salamanca, A., Almaini, O., Hartley, W. G., Lani, C., Mortlock, A., & Old, L. 2016, *ArXiv e-prints*
- Zheng, W., et al. 2004, *ApJS*, 155, 73
- Zheng, Z.-Y., Malhotra, S., Rhoads, J. E., Finkelstein, S. L., Wang, J.-X., Jiang, C.-Y., & Cai, Z. 2016, *ArXiv e-prints*
- Zheng, Z.-Y., et al. 2013, *MNRAS*, 431, 3589

APPENDIX

The spectroscopic redshifts used in the Field samples of galaxies (Section 3) came from the following sources (and references therein), as compiled by NED: Worseck et al. (2008); McIntosh et al. (2004); Noll et al. (2004); Le Fèvre et al. (2005) Bond et al. (2012); Balestra et al. (2010); Wuyts et al. (2008); Santini et al. (2009); Le Fèvre et al. (2004) Bonzini et al. (2012); Luo et al. (2008); Mainieri et al. (2008); Bond et al. (2011); Straughn et al. (2011) Mignoli et al. (2005); Xue et al. (2010); Trump et al. (2011); Treister et al. (2009); Hewett & Wild (2010); Wuyts et al. (2009) Tanaka et al. (2013); Eales et al. (2003); Barger et al. (2002); Menéndez-Delmestre et al. (2009); Reddy et al. (2006) Pope et al. (2006); Conselice et al. (2011); Pirzkal et al. (2013); Erb et al. (2006); Steidel et al. (2004); Papovich et al. (2001b) Fernández-Soto et al. (1999); Bertincourt et al. (2009); Fernández-Soto et al. (2001); Hayashi et al. (2009); Ly et al. (2009) Ramos Almeida et al. (2009); Whitaker et al. (2011); Park et al. (2010); Gobat et al. (2012, 2013, 2011) Kocevski et al. (2009); Erb et al. (2003); Shapley et al. (2005); Colbert et al. (2006) Keel et al. (2002); Steidel et al. (2003); Abraham et al. (2004); Vanzella et al. (2002); Wuyts et al. (2007); Kilic et al. (2005) Sealey et al. (1998); Galametz et al. (2013); Gavignaud et al. (2006); Worseck & Wisotzki (2006); Silverman et al. (2010) Szokoly et al. (2004); Elmegreen & Elmegreen (2010); Brammer et al. (2013); Trump et al. (2014); Kriek et al. (2008); Wolf et al. (1999) Doherty et al. (2010); Brusa et al. (2010); Söchting et al. (2012); Song et al. (2014) Pentericci et al. (2002); Kurk et al. (2004a); Pentericci et al. (2000); Croft et al. (2005); Kurk et al. (2004b); Roettgering et al. (1997) Lowenthal et al. (1997); Papovich et al. (2005); Moth & Elston (2002); Wang et al. (2004); Tadaki et al. (2011) Yoshikawa et al. (2010); Matsuda et al. (2011); Weiner et al. (2005); Georgakakis et al. (2006); Smail et al. (2004); Onodera et al. (2010) Shapley et al. (2004); Vogel & Reimers (1995); Peter et al. (2007); Chapman et al. (2004b); Moorwood et al. (2000) Cristiani & D'Odorico (2000); Stalin et al. (2010); Melnyk et al. (2013); Simpson et al. (2014); Donley et al. (2010); Casey et al. (2011) Salimbeni et al. (2009); Grazian et al. (2006); Rangel et al. (2014); Osmer et al. (1994) Silverman et al. (2005); Storrie-Lombardi et al. (1996); Dannerbauer et al. (2004); Cowie et al. (2004); Erb et al. (2004); Adams et al. (2011) Barger et al. (2000); Lowenthal et al. (2009); Phillips et al. (1997); Trouille et al. (2008); Swinbank et al. (2004) De Breuck et al. (2004); Anderson & Margon (1987); Digby-North et al. (2010); Erb et al. (2011); Harrison et al. (2012) Lehmer et al. (2009b); Petitjean & Srianand (1999); Hamann et al. (1997); York et al. (1991); Cowie et al. (1995) Zheng et al. (2004); Rodney et al. (2014); Yang et al. (2011); Donley et al. (2007); Georgantopoulos et al. (2011); Wirth et al. (2004) Dannerbauer et al. (2006); Kulas et al. (2012); Law et al. (2012); Dobrzycki & Bechtold (1996); Tripp et al. (1997) Tanner et al. (1996); Hainline et al. (2011); Schreier et al. (2001); Kirkpatrick et al. (2012); Brusa et al. (2009a); Bond et al. (2014) Daddi et al. (2005); van Breukelen et al. (2005); Knudsen et al. (2008); Bauer et al. (2002); Dawson et al. (2001) Fasano et al. (1998); Conselice et al. (2003); Riechers et al. (2011); Ivison et al. (2011); Wang et al. (2006); Barger et al. (2001b) Postman et al. (2001); Reimers et al. (1989); Iwata et al. (2005); Castro-Rodríguez & López-Corredoira (2012); Rafelski et al. (2011) Teplitz et al. (2007); Diener et al. (2013); Bothwell et al. (2013); Lanzetta et al. (1996); Campos et al. (1999); Coppin et al. (2008) Wolfe & Prochaska (2000); Bielby et al. (2013); Rafelski et al. (2009); Rigby et al. (2008); Akiyama (2005) Ross et al. (2012); Lilly et al. (2007); Sharp et al. (2002); Barger et al. (2001a); Rodríguez-Pascual et al. (1995); Simcoe et al. (2006) Venemans et al. (2007); McCarthy et al. (1996); Tapken et al. (2007); Santos et al. (2004); Vernet & Cimatti (2001) Songaila (1998); Sarajedini et al. (2011); Chapman et al. (2004c); Magdis et al. (2010); Fynbo et al. (2003b); Storrie-Lombardi & Wolfe (2000) Gavignaud et al. (2008); Cristiani et al. (2000); Feruglio et al. (2011); Shapley et al. (2001); Rottgering et al. (1995) Civano et al. (2011); Fynbo et al. (2001); Møller & Fynbo (2001); Stanford et al. (2004); Webb et al. (2003); Savaglio et al. (1997) Srianand (1996); Venemans et al. (2005); Le Fèvre et al. (1996); Maschietto et al. (2008); Ciardullo et al. (2012) Bond et al. (2010); Straughn et al. (2008); Xu et al. (2007); Lehmer et al. (2009a); Cantalupo et al. (2007); Lu et al. (1998) Trump et al. (2009); Grove et al. (2009); Barger et al. (2008); Petry et al. (1998); Tran et al. (2005) Sand et al. (2005); Hawkins & Veron (1993); Veron & Hawkins (1995); Inoue et al. (2011); Nestor et al. (2011); Shapley et al. (2006) Chapman et al. (2004a); Watabe et al. (2009); Hayashino et al. (2004); Steidel et al. (2000); Vanzella et al. (2004) Steidel et al. (1999); Mehlert et al. (2002); Ellison et al. (2001); de Bruyn et al. (1996); Polletta et al. (2008); Lemoine-Busserolle et al. (2010) Krumpel et al. (2008); Fiore et al. (2012); Vanzella et al. (2006); Tang et al. (2014); Gnerucci et al. (2011) Jangren et al. (2005); Boutsia et al. (2011); Hornschemeier et al. (2001); Barger et al. (2003); Hainline et al. (2006) Scott et al. (2000); Schaye et al. (2000); Ouchi et al. (2008); Vanzella et al. (2008) Fontanot et al. (2007); Tozzi et al. (2009); Brusa et al. (2009b); Patnaik et al. (1992); Saito et al. (2008) Shim et al. (2011); Vanzella et al. (2010); Rhoads et al. (2009); Daddi et al. (2009); Ouchi et al. (2004a) Yoshida et al. (2006); Savaglio et al. (1994); Schneider et al. (1991); Iwata et al. (2007); Tapken et al. (2006); Wang et al. (2009) Dawson et al. (2004); McLure et al. (2006); Ouchi et al. (2005); Saito et al. (2006); Maiolino et al. (2009) Hu et al. (2010); Ranalli et al. (2013); Zheng et al. (2013); Finkelstein et al. (2009a,b); Raiter et al. (2010) Stanway et al. (2007); Vanzella et al. (2005); Coppin et al. (2010); Pentericci et al. (2011); Bunker et al. (2004) Malhotra et al. (2005); Rhoads et al. (2005); Buchner et al. (2014); Hathi et al. (2008); Finlator et al. (2007); Stanway et al. (2004b) Dow-Hygelund et al. (2007); Finkelstein et al. (2011); Husband et al. (2013) Péroux et al. (2001); Djorgovski et al. (2003); Casey et al. (2012); Taniguchi et al. (2009); Martin et al. (2008); Henry et al. (2012) Murayama et al. (2007); Davies et al. (2010); Hu et al. (1996); Carilli et al. (2013); Elston et al. (1996) Wampler et al. (1996); Riechers et al. (2006); Kajino et al. (2009); Stark et al. (2013, 2011); Kakazu et al. (2007) Stern & Spinrad (1999); Weymann et al. (1998); Dawson et al. (2002); Neri et al. (2014); Reshetnikov & Vasil'Ev (2002) Spinrad et al. (1998); Ando et al. (2004); Tan et al. (2014); Kashikawa et al. (2011); Shimasaku et al. (2006); Toshikawa et al. (2014) Jiang et al. (2013); Nagao et al. (2007); Dawson et al. (2007); Lemaux

et al. (2009); Anderson et al. (2001) Hu et al. (2004, 1999); Curtis-Lake et al. (2012); Ouchi et al. (2010); Grazian et al. (2012); Ouchi et al. (2009) Schenker et al. (2012); Ono et al. (2012); Stanway et al. (2004a); Jiang et al. (2011); Taniguchi et al. (2005) Kashikawa et al. (2006); Iye et al. (2006); Nagao et al. (2004, 2005); Rhoads et al. (2004)